Lehigh University
Lehigh Preserve

Theses and Dissertations

1989

DC characterization of electron irradiated depletion mode heterojunction FETs /

S. B. Witmer
Lehigh University

Follow this and additional works at: https://preserve.lehigh.edu/etd

Part of the Electrical and Computer Engineering Commons

Recommended Citation

Witmer, S. B., "DC characterization of electron irradiated depletion mode heterojunction FETs /" (1989). *Theses and Dissertations*. 4977.
https://preserve.lehigh.edu/etd/4977

This Thesis is brought to you for free and open access by Lehigh Preserve. It has been accepted for inclusion in Theses and Dissertations by an authorized administrator of Lehigh Preserve. For more information, please contact preserve@lehigh.edu.

DC CHARACTERIZATION OF ELECTRON IRRADIATED DEPLETION MODE HETEROJUNCTION FETs

by

S.B. Witmer

A Thesis
Presented to the Graduate Committee
of Lehigh University
in Candidacy for the Degree of
Master of Science
in
Electrical Engineering

This thesis is accepted and approved in partial fullfillment of the requirements for the degree of Master of Science in Electrical Engineering.

Dec. 12, 1988
(date)

D. R. Decker
Professor in Charge

L. J. Varnerin
Chairman of Department

CONTENTS

LIST OF FIGURES

ABSTRACT

Heterojunction FETs were irradiated with 2.5MeV electrons and the changes in the DC device characteristics were investigated. The electron fluence ranged from $6.75X10^{14}cm^{-2}$ to $6X10^{15}cm^{-2}$. Total dose induced charge build-up in the GaAs region due to the filling of radiation induced traps was the primary mechanism that degraded the DC characteristics. Numerical calculations of the charged traps in the GaAs are used to predict the threshold voltage shifts which compare well to the measured results.

The experimental results show that the threshold voltage becomes more positive after irradiation which in turn reduces the drain current. It is shown that at high electron fluence levels ΔV_{th} is the dominant cause in the reduction of the drain current. The peak transconductance of the 2DEG was also reduced. The reverse gate leakage current increased slightly after irradiation.

1. INTRODUCTION

High speed digital circuits have been designed in GaAs. These circuits are increasingly being used in radiation environments such as in space and military applications. The AlGaAs/GaAs heterojunction transistor is currently being used to design digital high speed memory circuits by Bell Laboratories. The effects of radiation on heterojunction transistors (HFETs) have not been fully characterized.

A radiation environment is the most demanding ambient for semiconductor circuits. Neutrons, protons, gamma rays, and electrons affect the operation of devices and circuits by causing ionization and lattice damage. There are three major categories of radiation testing: transient or dose rate testing, single event upset (SEU) testing, and total dose testing. SEU testing and transient testing measures the effects of ionization induced by single heavy ions and pulses of electrons respectively. Total dose testing measures the degradation in devices and circuits from long term radiation exposure. Total dose induced charge build-up is the primary failure mechanism in circuits that operate in space radiation environments. The total dose effects are caused by lattice damage produced by high energy electrons and protons trapped in the earths magnetosphere and from cosmic rays. [8] The total dose effects in GaAs HFETs from space electron irradiation can be simulated by exposing the devices to electrons from a Van de Graaff accelerator.

This paper evaluates total dose effects of electron irradiation on HFETs. First the HFET device physics is discussed in section 2. Then Total dose electron radiation effects in GaAs and AlGaAs are discussed in section 3. Section 4 describes the experimental procedure and includes details of the test set-up, Van de Graaff accelerator, and device processing and geometry. The experimental results and analysis of results are presented in section 5.

2. HFET PHYSICS

2.1 Two Dimensional Electron Gas

The HFET structure is based on the formation of a heterojunction interface between N^+ AlGaAs and undoped GaAs. A thin high density layer of electrons (2DEG) is present on the GaAs side of the AlGaAs/GaAs interface. The 2DEG electrons accumulate at the interface when electrons diffuse from the

N$^+$ AlGaAs region into the GaAs region until the Fermi levels of the AlGaAs and GaAs are equal. Due to the band gap discontinuity at the interface a potential well is formed in the undoped GaAs. Figure 1 show the interface at equilibrium.

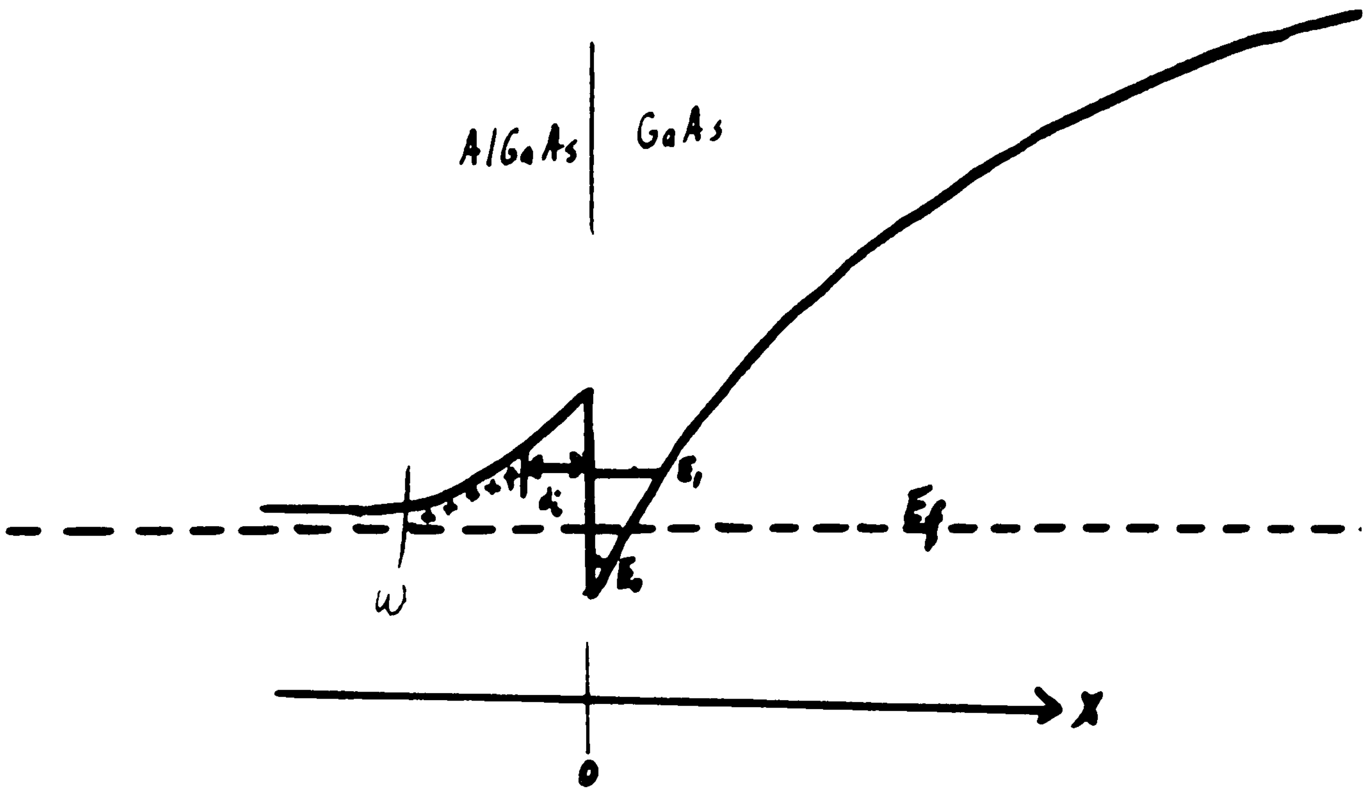

Figure 1. AlGaAs/GaAs interface in equilibrium

The electron surface charge density, n_s , can be calculated by solving Schrodinger's equation (Eq.1).

$$\frac{h^2}{2m^*}\frac{\partial^2\phi_i}{\partial x^2}+\left[E_i-V(x)\right]\phi_i=0 \tag{1}$$

where m^* is the electron effective mass, ϕ_i is the probability density function, E_i is the quantized energy of the ith subband and V(x) is the potential function. V(x) satisfies Poisson's equation, Eq.2.

$$\frac{\partial V\left[x\right]}{\partial x}=\frac{q\rho\left[x\right]}{\varepsilon} \tag{2}$$

where $\rho(x)$ is the space charge density in the GaAs region. The space charge is the sum of the conduction band electrons and the charged acceptors and donors. $\rho(x)$ can be expressed as:

$$\rho(x)=q(N^{+D}-N^{-A})-q\sum_{i=0}^{\infty}n_i\left|\phi(x)\right|^2 \tag{3}$$

where

$$n_i=\frac{m^*K_BT}{\bar{h}^2}\ln\left\{1+\exp\left[\frac{q(E_f-E_i)}{K_BT}\right]\right\} \tag{4}$$

In Equation 3, N^+_D and N^-_A are the ionized donor and acceptor densities in the GaAs respectively. In

equation 4, E_f is the Fermi level and K_B is the Boltzmann constant.

The calculation of n_s can be simplified by approximating $V(x)=F_sX$ for $X>0$ and $V(X)=\infty$ for $X<0$ where F_s is the electric field at the interface. The solution to Schrodinger's equation using this approximation yields the well known Airy's equation (Eq. 5) for the quantized energy states.

$$E_i=\left(\frac{\bar{h}^2}{2m^*}\right)^{\frac{1}{3}}\left[3qF_s\pi\frac{\left(i+\frac{3}{4}\right)}{2}\right]^{\frac{2}{3}} \tag{5}$$

By substituting $F_s=\frac{qn_s}{\varepsilon}$ into the Airy's equation, the first two quantized energy levels can be expressed as $E_0=\zeta_0 n_s^{\frac{2}{3}}$ and $E_1=\zeta_1 n_s^{\frac{2}{3}}$. ζ_0 and ζ_1 have been determined experimentally and have the following value: $\zeta_0=2.5\text{x}10^{-12}\text{Vm}^{\frac{4}{3}}$, $\zeta_1=3.2\text{x}10^{-12}\text{Vm}^{\frac{4}{3}}$. By cyclotron effective mass measurements, the two-dimensional density of states is $D=\frac{qm^*}{\pi\bar{h}^2}\approx 3.24\text{x}10^{17}\frac{m^{-2}}{V^{-1}}$. n_s can be written as [10]

$$n_s\approx\frac{DK_BT}{q}\sum_{i=0}^{1}\ln\left\{1+\exp\left(\frac{q\left(E_f-E_i\right)}{K_BT}\right)\right\}. \tag{6}$$

Expanding equation 6 for the first two subbands,

$$n_s=\frac{DK_BT}{q}\ln\left[\left(1+\exp\left(\frac{q(E_f-E_0)}{K_bT}\right)\right)\left(1+\exp\left(\frac{q(E_f-E_1)}{K_BT}\right)\right)\right] \tag{7}$$

2.2 *Calculation of* E_{fo}, *Equilibrium Fermi Level at the Interface*

At equilibrium the Fermi level in the GaAs and AlGaAs are equal. Equation 7 gives the relationship between n_s and E_f. By integrating Poisson's equation from the interface, x=0 to the depletion width edge in the AlGaAs, $w=\frac{n_s}{N_D}+d_i$, the following Equation is obtained: [4]

$$n_s\approx -d_iN_D+\sqrt{\frac{2\varepsilon N_D}{q}\left(\Delta E_c-E_{f2}-E_{f1}\right)+N_d^2d_i^2} \tag{8}$$

where E_{f2} and E_{f1} are the Fermi levels referenced with respect to the conduction band in the AlGaAs and GaAs respectively. The numerical solution of equation 7 and equation 8 yields E_{fo}. A plot of equation

7 is shown in figure 2. For n_s between $5\text{x}10^{11}\frac{1}{\text{cm}^2}$ to $1.5\text{x}10^{12}\frac{1}{\text{cm}^2}$, n_s Versus E_f is almost linear. The curves can be approximated by :

$$E_{fo} \approx \Delta E_{fo}(T) + a n_s \tag{9}$$

where $\Delta E_{fi}(T)=0$ for T=300 K.

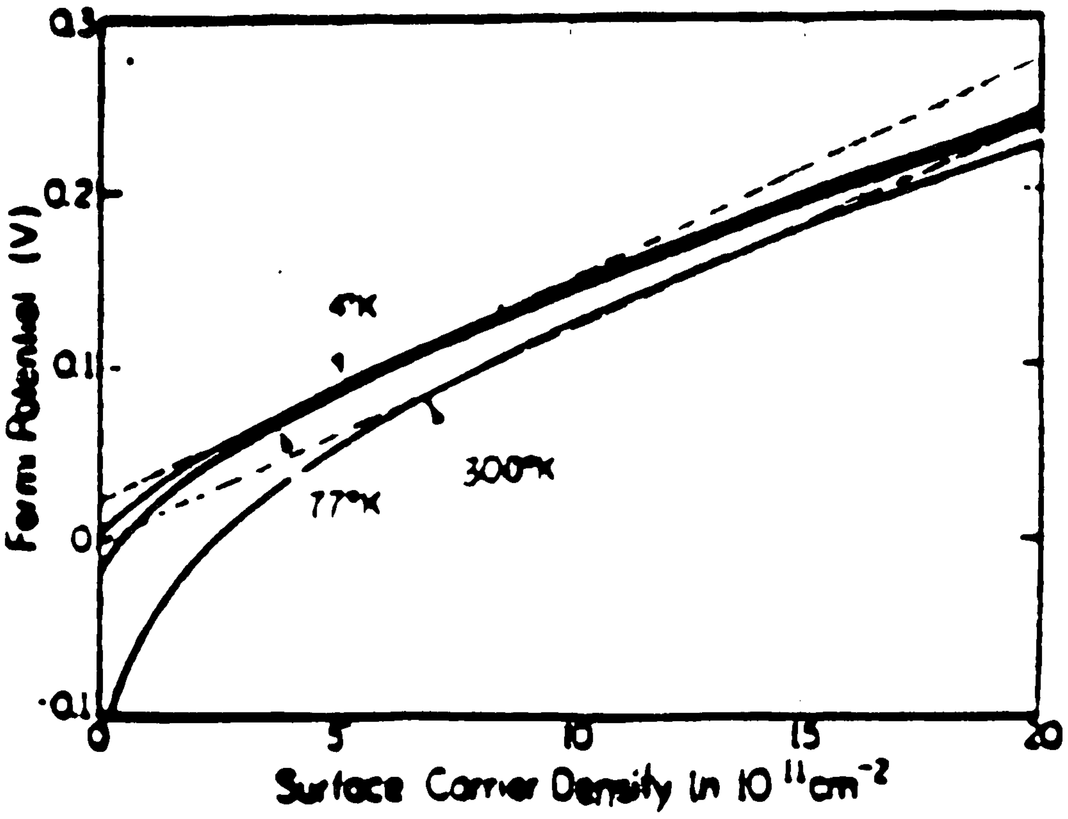

Figure 2. Fermi level versus surface carrier density, n_s at 300, 77, and 4 K, respectively. Linear approximations are shown as dashed lines.

An analytical expression for E_{fo} can be derived by substituting equation 9 into equation 8 and solving the quadratic equation in terms of E_{fo}. The solution yields:

$$E_{fo} \approx \frac{-B+\sqrt{B^2-4AC}}{2A}$$

$$\text{where} \quad A=\frac{1}{a^2}, \quad B=\frac{2N_D d_i}{a}+\frac{2\varepsilon_{AlGaAs}N_D}{q}, \quad C=\frac{2\varepsilon_{AlGaAs}{}^*N_D}{q}\left(\frac{\phi_m}{q}-\frac{\Delta E_c}{q}\right) \tag{10}$$

2.3 *Charge Control*

The 2DEG concentration can be controlled if a Schottky contact is made to the AlGaAs. Charge control takes place when the Schottky junction depletion region overlaps the AlGaAs/GaAs heterojunction depletion region. If a negative gate bias is applied so that the AlGaAs region is totally depleted, then by integrating the electric field from the interface to the gate the charge control equation can be derived (eq. 11). For the AT&T depletion mode HFET structure shown in figure 3 the integration yields:

$$v_2=\frac{-qN_D d_d^2}{2\varepsilon_{AlGaAs}}+\frac{Q_{GaAs-2}}{\varepsilon_{AlGaAs}}\left[d_d+w_{02}+w_i+W_{02}'\right]+\frac{Q_{GaAs-2}}{\varepsilon_{GaAs}}\left[w_{01}+W_{01}'\right]-\frac{qN_d d_d}{\varepsilon_{GaAs}}\left[w_{01}+W_{01}'\right]\ldots.$$
$$-\frac{qN_d d_d}{\varepsilon_{AlGaAs}}\left[w_{02}+W_{02}'\right]+\frac{\Delta E_c}{q} \qquad (11)$$

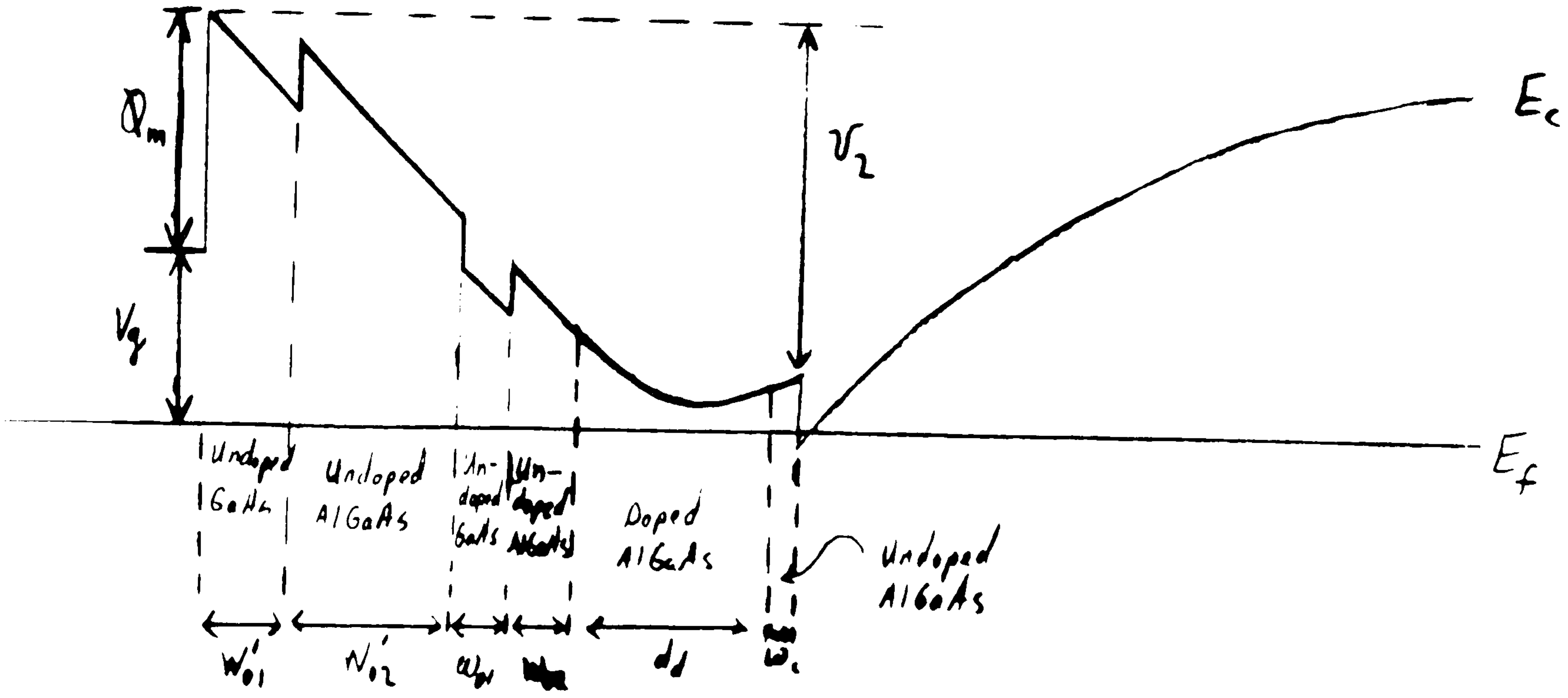

Figure 3. Band diagram of AT&T depletion mode HFET structure with a negative gate bias applied.

Q_{GaAs-2} in equation 11 is the surface charge density at the AlGaAs/GaAs interface. Solving for Q_{GaAs-2} in equation 11 yields:

$$Q_{GaAs-2}=\frac{1}{\frac{1}{\varepsilon_{AlGaAs}}\left[d_d+w_i+w_{02}+W_{02}'\right]+\frac{1}{\varepsilon_{GaAs}}\left[w_{01}+W_{01}'\right]}\left[-V_p+v_2\right].$$

where $$V_p=\frac{-qN_D d_d^2}{2\varepsilon_{AlGaAs}}-\frac{qN_D d_d\left[w_{02}+W_{02}'\right]}{\varepsilon_{AlGaAs}}-\frac{qN_D d_d\left[w_{01}+W_{01}'\right]}{\varepsilon_{GaAs}}+\frac{\Delta E_c}{q} \qquad (12)$$

Q_{GaAs-2} in equation 12 can be written as the sum of the 2DEG surface charge, n_s and the ionized impurity and trapped sheet charge, $Q_{GaAs-2}=q\,n_s+Q_{IT-2}$. By using the following substitutions:

1. $\varepsilon_{GaAs}=\varepsilon_{AlGaAs}=\varepsilon_{ave}=\dfrac{\varepsilon_{GaAs}\left[w_{01}+W_{01}'\right]+\varepsilon_{AlGaAs}\left[w_i+w_{02}+W_{02}'+d_d\right]}{d_{TOT}}$

2. $d_1=w_{01}+W_{01}'+w_{02}+W_{02}'$

3. $d_2=d_1+d_d$

4. $d_{tot}=d_2+w_i$

5. $v_2=V_g-\phi_m+\Delta E_c-E_f$

equation 12 can be simplified (eq. 13).

$$n_s=\frac{\varepsilon_{ave}}{q\, d_{TOT}}\left[V_g-V_{off}\right] \tag{13}$$

where $V_{off}=\phi_m+E_{f-off}+\frac{Q_{I-T}\, d_{TOT}}{\varepsilon_{ave}}-\frac{qN_D}{2\varepsilon_{ave}}\left[d^2{}_2-d^2{}_1\right]$. V_{off} is the gate voltage required to annihilate the 2DEG charge, n_s. The threshold voltage can be found by substituting V_{off} into equation 13, replacing V_g and E_f with V_{th} and E_{f-th} respectively, and then solving for V_{th}. V_{th} can be expressed as: [7]

$$V_{th}=\phi_m+E_{f-th}+d_{tot}\frac{Q_{GaAs-2}}{\varepsilon_{ave}}-qN_D\frac{\left[d_2{}^2-d_1{}^2\right]}{2\varepsilon_{ave}} \tag{14}$$

2.4 Current versus Voltage Characteristics

The current/voltage characteristics for the HFET have been derived by Park and Kwack. The derivation starts with the current density equation (eq.15).

$$I=w\left[\mu E_s Q_s+D_n\frac{\partial Q_s}{\partial y}\right] \tag{15}$$

In equation 15, Q_s is the mobile surface charge density and equals qn_s, D_n is the diffusion coefficient for GaAs, E_s is the electric field in the y direction in the 2DEG and w is the gate width. Using the Einstein relationship, $\frac{D}{\mu}=\frac{KT}{q}$, equation 15 can be rewritten as (see fig.4):

$$I=-w\mu\left[E_s Q_s+\frac{KT}{q}\frac{\partial Q_s}{\partial y}\right] \tag{16}$$

The mobility versus electric field characteristics can be approximated by the following equation:

$$\mu(E)=\frac{\mu_o}{1+\frac{1}{E_s}\frac{\partial V}{\partial y}} \tag{17}$$

Combining equations 15, 16, and 17 yields:

$$I=\frac{w\mu_o\varepsilon_{GaAs}}{d_{TOT}}\frac{\left[V_g-V_{off}+\frac{KT}{q}-V(y)\right]\frac{\partial V}{\partial y}}{1+\frac{1}{E_s}\frac{\partial V}{\partial y}} \tag{18}$$

The boundary conditions are:

1. $V(y=0)=R_s I$
2. $V(y=L)=V_D-R_D I=V_D-R_s I$

where R_s and R_D are the source and drain series resistances. Integrating equation 18 and using the above boundary conditions yields equation 19, the current/voltage relation for $V_D \leq V_{sat}$. V_{sat} is defined as the drain voltage at which the electric field at y=L equals E_{sat}, where E_{sat} is the electric field at which the electrons are moving at the saturation velocity. [2]

$$I=\frac{E_s L}{4R_s}\left[\left(\frac{V_D}{E_s L}+2\alpha\beta R_s-\alpha R_s V_D+1\right)-\sqrt{\left(\frac{V_D}{E_s L}+2\alpha\beta R_s V_D+1\right)^2-\frac{8\alpha R_s}{E_s L}\left(\beta V_D-\frac{V_D{}^2}{2}\right)}\right]$$

$$\alpha=\frac{w\mu_o\varepsilon_{GaAs}}{dL} \qquad \beta=V_g-V_{off}+\frac{KT}{q} \tag{19}$$

The current/voltage relationship for $V_{DS}>V_{sat}$ has also been derived by Park and Kwack. The derivation starts by writing Poisson's equation in the y direction at the drain end in the 2-D gas region.

$$\frac{\partial^2 V}{\partial y^2}=\frac{Q_s}{\varepsilon_{GaAs}}=\frac{1}{\varepsilon_{GaAs}}\frac{J}{v_s}=\frac{I_s}{v_s\varepsilon w d_o} \tag{20}$$

In equation 20, I_s is the saturation current, w is the gate width and d_o is the 2DEG layer width.

The reasoning behind the formulation of Poisson's Equation is depicted in figure 4. Figure 4 shows the field and charge coupling for $V_{DS}>V_{sat}$ in the 2DEG and AlGaAs. The x directional electric field component gets small as $y \rightarrow L-\Delta L$ in the 2DEG region while the y component gets larger. At $y=L-\Delta L$ the field is approximately equal to E_{sat} and the AlGaAs is totally depleted. The positive ionic charge in the AlGaAs is coupled to negative charge on the gate. There is no coupling between the AlGaAs positive charge and the 2DEG negative charge for $L-\Delta L<X<L$ and hence only the y component of electric field is present in this region. The negative charge in this region is assumed to form a dipole with positive space charge under the drain contact. Therefore the one-dimensional Poisson's equation

takes the form of equation 20 where the charge density, $Q_s=\frac{I_s}{v_s d_o w}$.

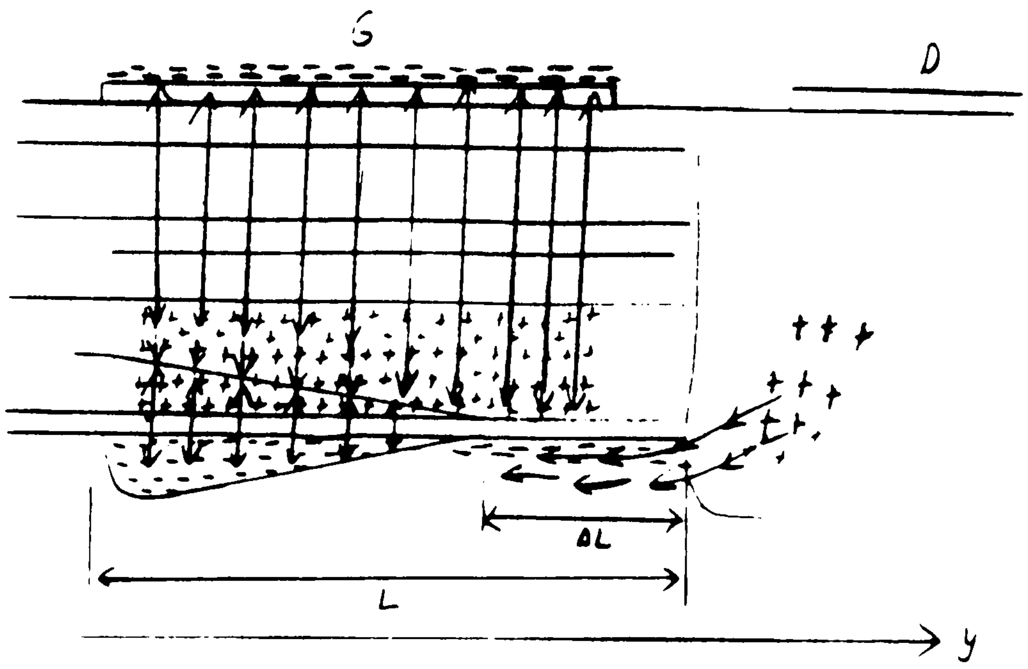

Figure 4. Electric fields in the 2DEG for $V_d \geq V_{d-sat}$

The boundary conditions in the saturation region are:

1. $V(y=0)=V_{DS}-R_D I_s$
2. $V(y=\Delta L)=V_D-R_D I_s$

where V_{DS} is the drain voltage when saturation occurs. The solution to equation 20 yields :

$$V_D=V_{DS}+\frac{I_s}{2wd_o\varepsilon_{GaAs}v_s}\Delta L^2-E_s\Delta L \tag{21}$$

By using the approximation $I_{DS} \propto \frac{V_{ds}}{L-\Delta L}$, the ratio of $\frac{I_s}{I_{DS}}$ can be expressed as:

$$\frac{I_s}{I_{DS}}\approx\frac{L}{L-\Delta L} \tag{22}$$

Substituting equation 22 into equation 21 yields:

$$V_D=V_{DS}+\frac{I_s L^2}{2wd_o\varepsilon_2 v_s}\left(1-\frac{I_{DS}}{I_s}\right)^2-E_s L\left(1-\frac{I_{DS}}{I_s}\right) \tag{23}$$

$I_s=I_{DS}$ when the drain voltage, V_D equals the pinch-off voltage, $\approx V_{DS}$. Therefore V_{DS} and I_{DS} can be obtained by taking the derivative of equation 19 with respect to V_D and setting it equal to zero. Solving for V_D yields the saturation voltage V_{DS} . Then V_{DS} and I_{DS} are used in equation 23 to obtain the current/voltage relationship in the saturation region. [2]

3. *TOTAL DOSE RADIATION EFFECTS IN GaAs AND AlGaAs*

3.1 *Lattice Damage and Traps in GaAs and AlGaAs*

High energy radiation can cause permanent damage to the crystalline structure of the device. The permanent defects consist of dislocated lattice atoms such as vacances, divacancies, and interstitial pairs. High energy particles can also cause damage regions of various sizes consisting of defect clusters and spike zones of quasi-metallic behavior.

The displaced atoms give rise to additional energy levels in the band gap of the semiconductors. These energy levels can act as recombination or generation centers. In addition, the defects trap mobile charge and hence reduce the free carrier concentration. Electron traps are like acceptor states but are located above the intrinsic level and hole traps are like donor states but are located below the intrinsic level. The traps remove carriers from the conduction band and valence band causing the material to look more intrinsic (carrier removal).

Deep level transient spectroscopy measurements of 1MeV irradiated GaAs have been reported by Lang et al. , Pones et al., and Li et al. Five deep electron traps and five deep hole traps have been identified. The introduction rates $\left[\frac{\text{\# of Traps}}{\text{Electron Fluence}}\right]$ and capture cross-sections have been obtained for each hole & electron trap. Table 1 summarizes the results for 1 MeV electron irradiated GaAs. [3]

Experimental measurements of the carrier removal rate, $\frac{\Delta n}{\phi}$ versus incident electron energy has been made by Grimshaw and Banbury et al. Their data fits the theoretical calculations based on Rutherford scattering for a threshold displacement energy of 17eV. The theoretical calculations predict that 2.5MeV electrons will produce approximately 2X more damage than 1MeV electrons. Therefore the 1MeV introduction rates must be scaled by a factor of 2 for calculations based on 2.5MeV electron irradiation.

Deep level transient spectroscopy measurements of $Al_xGa_{1-x}As$ show trap levels similar to those found in GaAs. The energy levels of the traps shift smoothly with the semiconductor band gap as the Aluminum fraction , x, is varied. Figure 5, shows the shift of the three major electron traps with increasing Al. fraction. All levels except E_3 have the same relative shift $\frac{E(x)}{E_0}$ with x as the band gap.

The E_3 level is fixed relative to the valence band. This can be taken as strong evidence that the E_3 level is a vacancy. Work done by M Jaros and S. Brand shows that for GaAs, one should expect vacancy states to be strongly tied to the valence band. [6]

TABLE 1: Energy levels,capture cross-section, and introduction rates of 1-MeV irradiated GaAs.

Traps	Energy level E_t(eV)	Capture cross-section σ(cm^2)	Introduction rate I_t(cm^{-1})
E1	E_c–.0.08	σ=10^{-17}	1.8
E2	E_c–0.14	σ=1.2X10^{-15}	2.8
E3	E_c–0.35	σ=6.2X10^{-15}	0.3
E4	E_c–0.71	σ=2.2X10^{-13}	.07
E5	E_c–0.90	σ=5.8X10^{-14}	0.1
H1	E_v–0.13	σ=5.9X10^{-18}	0.22
H2	E_v–0.29	σ=5.9X10^{-18}	0.70
H3	E_v–0.35	---	.08
H4	E_v–0.44	σ=9.0X10^{-15}	0.30
H5	E_v–0.71	σ=2.3X10^{-13}	0.30

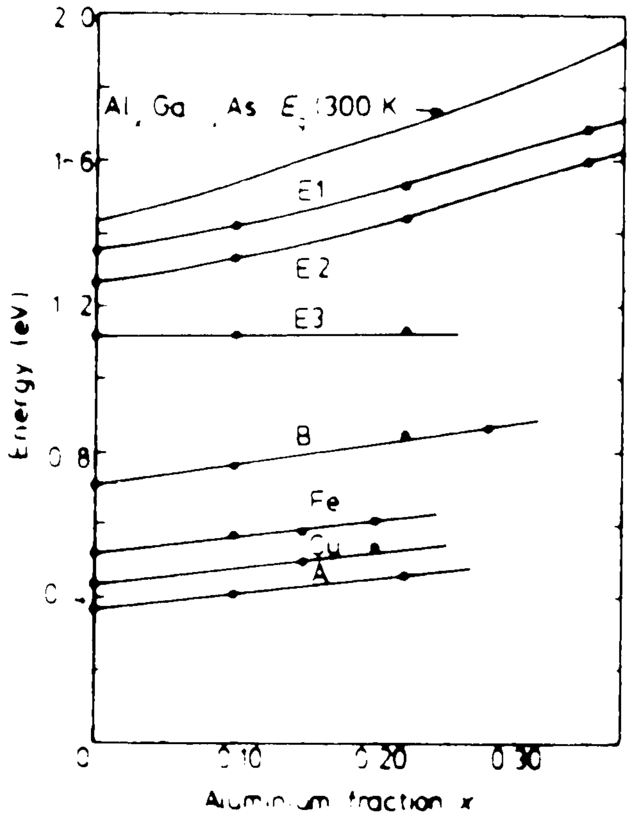

Figure 5. Energy level shifts of deep levels in $Al_xGa_{1-x}As$ as a function of Al mole fraction x.

3.2 Degradation of Low Field Mobility and Saturation Velocity

The depletion mode HFETs are generally used as resistive components in inverter circuits (DCFL,SFFL) configured with the gate and source tied together. The speed of the inverter depends mostly on the turn-on/turn-off speed of the E-HFETs and not in the D-HFETs but the output voltage swing of the inverter depends on the D-HFETs resistance in the saturation region. Therefore in digital circuits the degradation in the saturation velocity in D-HFETs is more important than the low field mobility since it increases the D-HFET channel resistance which reduces inverter output voltage swing.

The electron irradiation decreases the saturation velocity and low field mobility by inducing charged trapping centers which increase coulombic scattering in the 2DEG. [8]

3.3 Radiation Induced Charge Build-up in D-HFETs

The band diagram of a depletion mode HFET with Vg=Vth is shown in figure 8. At threshold the Fermi level is close to the conduction band edge at the AlGaAs-GaAs interface. The amount of charge from the AlGaAs required to bend the GaAs conduction band edge at the interface close to the Fermi level, depends on the trap density and energy distribution of the traps in the GaAs region. When electron traps exist in the GaAs bandgap, electrons normally available for conduction in the conduction band become trapped. The existence of traps requires the AlGaAs to contribute more electrons to the GaAs before conduction can occur at the interface. This required additional negative charge contributes to the threshold shift. The electric field at the interface increases due to the increased GaAs charge, which in turn, causes the quantized energy levels in the quantum well to increase. [7]

The space charge in the AlGaAs region can also be altered by the introduction of radiation induced traps. At threshold the gate is negatively biased and the N^+ AlGaAs region is depleted. Essentially all the electron traps above the Fermi Level are neutral and all hole traps below the Fermi level are also neutral. The traps in the depleted region contribute only a small amount of additional space charge. For this reason most of the threshold voltage shift comes from the filled traps in the GaAs region. The change in the threshold voltage due to the presence of traps has been investigated in both the AlGaAs and GaAs region.

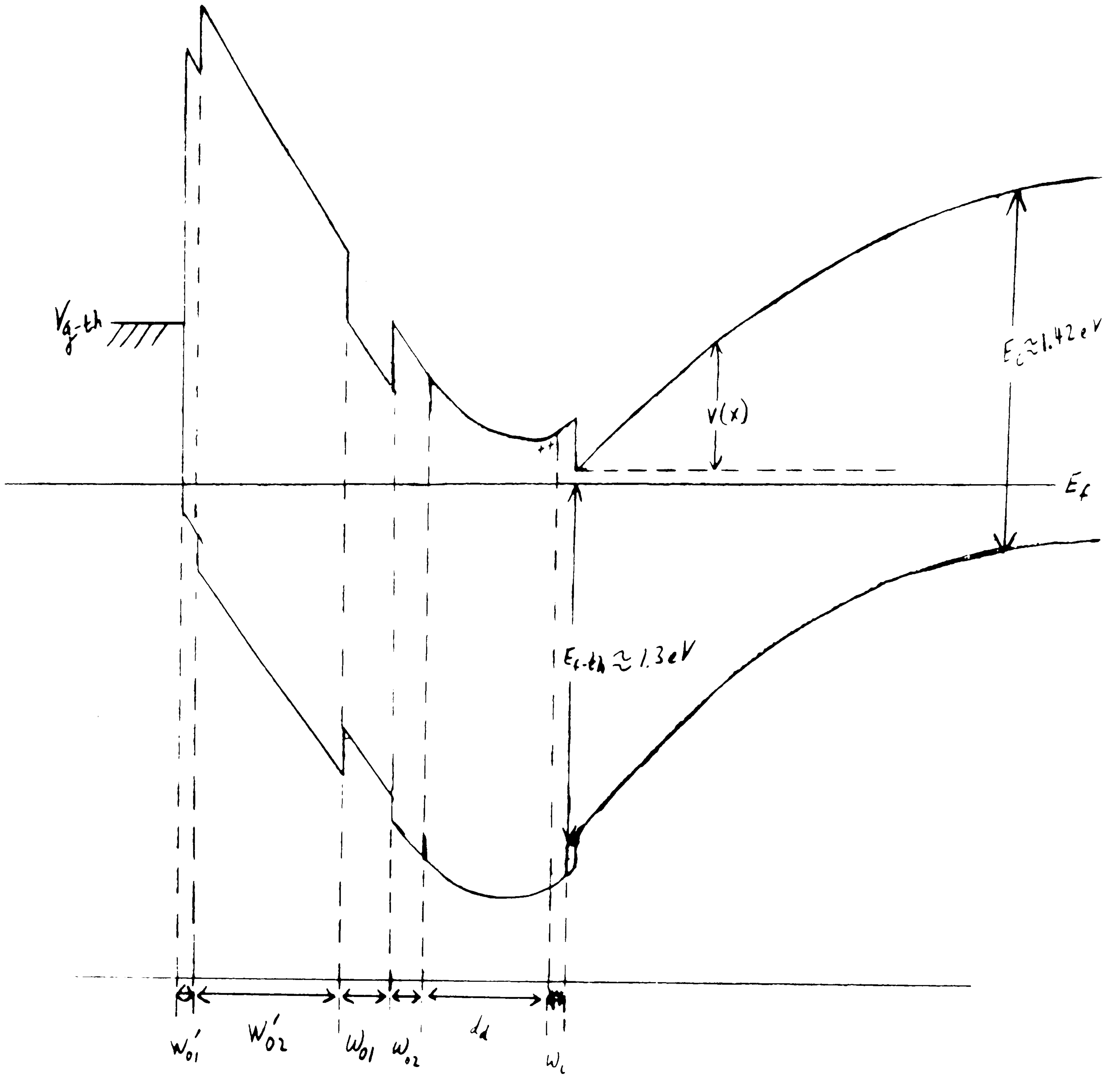

Figure 6. Band diagram of depletion mode HFET with $V_g=V_{th}$

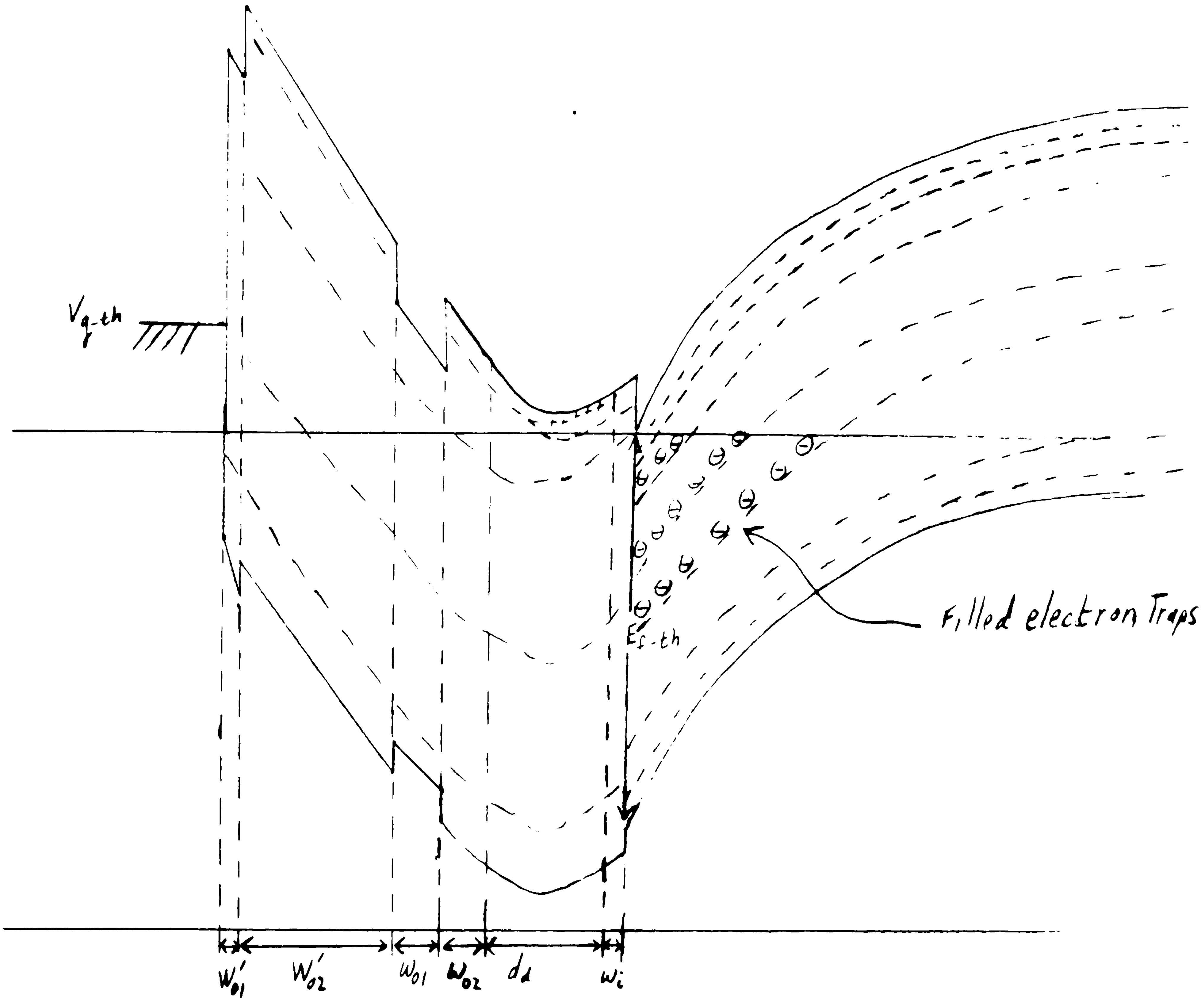

Figure 7. Band diagram of the AT&T HFET with $V_g=V_{th}$ with radiation induced traps.

3.3.1 Analytical Expression for ΔV_{th} **The threshold voltage for the AT&T HFET developed in section 2 can be written in a more general form as follows:**

$$V_{th} \approx \phi_m + E_{f-th} + \frac{Q_{GaAs-2} d_{TOT}}{\varepsilon_{ave}} - \left[\int_0^{gate} \left[\int_0^{x} \frac{Q(x')}{\varepsilon_{ave}} dx' \right] dx \right]. \qquad (26)$$

From the above equation, the change in the threshold voltage due to electron fluence is:

$$\Delta V_{th} \approx \Delta E_{f-th} + \frac{\Delta Q_{GaAs-2} d_{TOT}}{\varepsilon_{ave}} - \Delta \left[\int_0^{gate} \left[\int_0^{x} \frac{Q(x')}{\varepsilon_{ave}} dx' \right] dx \right]. \qquad (26)$$

In equation 26, Q(x') is the space charge density in the region from gate to the AlGaAs/GaAs interface and ε_{ave} is the average permittivity of the GaAs and AlGaAs. The GaAs & AlGaAs thicknesses are used as weighting factors in the averaging (eq. 27).

$$\varepsilon_{ave} = \frac{\varepsilon_{GaAs} \left(w_{01} + W'_{01}\right) + \varepsilon_{AlGaAs} \left(w_i + w_{02} + W'_{02} + d_d\right)}{d_{TOT}}.$$

$$\text{where} \quad d_{TOT} = w_{01} + W'_{01} + w_i + w_{02} + W'_{02} + d_d \qquad (27)$$

The barrier height, ϕ_m, is assumed not to be effected by the radiation and therefore does not show up in equation 26. The integral term in equation 25 just yields the last term in equation 14 in section (2.3). before irradiation. Q_{GaAs-2} is the total surface charge density ($\frac{coul}{cm^2}$) at the AlGaAs-GaAs interface. Q_{GaAs-2} has a strong dependence on the energy level and density of the traps in the GaAs region. At threshold the Fermi level is close to the conduction band at the interface, and the electron traps below the Fermi level are negatively charged.

3.3.2 ΔV_{th} *Due to Radiation Induced Traps in the* GaAs Region: " As shown in equation 26, the change in the net negative space charge in the GaAs due to the radiation induced traps is directly related to the threshold voltage shifts. The change in the net negative charge in the GaAs region can be calculated by solving Poisson's equation from the AlGaAs-GaAs interface into the bulk GaAs. From the solution of Poisson's equation before and after irradiation ΔQ_{GaAs-2}, can be calculated.

Poisson's equation can be written in one dimension x, where x is the spatial dimension perpendicular to the AlGaAs/GaAs interface as follows:

$$\frac{d^2V(x)}{dx^2}=\frac{Q_{GaAs-3}(x)}{\varepsilon_{GaAs}} \tag{28}$$

In equation 28, V(x) is the potential difference relative to the interface (see fig.8), and Q_{GaAs-3} is the space charge density (coul./cm^3) in the GaAs region. ε_{GaAs} is the permittivity of GaAs. In the presents of radiation induce traps, $Q_{GaAs-3}(x)$ can be written as shown in equation 29.

$$\begin{aligned}Q_{GaAs-3}(x)=&-q^*N_c f(E_c-E_f)-q^*\phi\sum I_{t-e}{}^*f(E_{t-e}-E_f)+q^*N_v f(E_v-E_f)+\cdots\\&q^*\phi^*\sum I_{t-h}{}^*f(E_{t-h}-E_f)+q^*N_D f(E_D-E_f)-q^*N_A{}^*f(E_A-E_f)\end{aligned} \tag{29}$$

Table 2 defines the variables used in equation 29.

TABLE 2: Definitions of variables used in equation 29

Variable	Definition	
N_c	Effective density of states in the conduction band	
N_v	Effective density of states in the valence band	
N_D	Background donor density	
N_A	Background acceptor density	
E_v	Energy level of valence band	
E_c	Energy level of conduction band	
E_{t-e}	Energy level of electron traps	
E_{t-h}	Energy level of hole trap	
E_A	Energy level of acceptors states	
E_D	Energy level of donors states	
E_f	Fermi level	
I_{t-h}	Introduction rate of hole traps	
I_{t-e}	Introduction rate of electron traps	

Since the Fermi level is flat in the GaAs region, $E_f(x)$ relative to the valence band can be expressed as $E_{fo}-V(x)$ where E_{fo} is the Fermi level at the interface relative to the valence band of the GaAs. At threshold, the Fermi level at the interface is defined as, $E_{fi-th}\approx 1.3$eV, which has been determined from numerical simulation studies in AT&T D-HFETs. Eliminating $E_f(x)$ from equation 29, Poisson's equation can be expressed in the GaAs region as follows:

$$\frac{d^2V(x)}{dx^2}=\left(\frac{1}{\varepsilon_{GaAs}}\right)-q^*N_c f(E_g-E_{fo}+V(x))-q^*\phi\sum I_{t-e}{}^*f(E_{t-e}-(E_{fo}-V(x)))+q^*N_v f(E_v-(E_{fo}-V(x)))+\ldots\ldots$$
$$q^*\phi^*\sum I_{t-h}{}^*f(E_{t-h}-(E_{fo}-V(x)))+q^*N_D f(E_D-E_f)-q^*N_A{}^*f(E_A-E_f). \qquad (30)$$

The boundary conditions are $V(x)=0$ at the AlGaAs-GaAs interface, which corresponds to $x=0$ in figure 8 and $V(x)=\frac{E_{fo}-E_{fB}}{q}$ at $x=\infty$ where E_{fB} is the Fermi level in the bulk GaAs. E_{fB} is can be found from Fermi-Dirac Statistics using the condition of space charge neutrality in the bulk (eq. 31).

$$Q_{GaAs-3}(x=\infty)=-q^*N_c f(E_c-E_{fB})-q^*\phi\sum I_{t-e}{}^*f(E_{t-e}-E_{fB})+q^*N_v f(E_v-E_{fB})+\cdots$$
$$q^*\phi^*\sum I_{t-h}{}^*f(E_{t-h}-E_{fB})+q^*N_D f(E_D-E_{fB})-q^*N_A{}^*f(E_A-E_{fB})=0 \qquad (31)$$

$V(x)$ and Q_{GaAs-2} can be solved for numerically with the aid of a desk top computer. The GaAs region is divided up into incremental sections of thickness Δx_n. A recursive equation for ΔV_n can be written as follows:

$$\Delta V_n=\frac{Q'_{GaAs-2_{n-1}}\Delta X}{\varepsilon_{GaAs}}+\frac{Q'_{GaAs-3_{n-1}}\Delta X^2}{2\varepsilon_{GaAs}}$$

$$\text{where}\quad Q'_{GaAs-2_n}=\sum_0^n Q'_{GaAs-3_n}\Delta X_n \qquad V_n=\sum_1^n \Delta V_n$$

$$\text{and}\quad \Delta V_0=0 \qquad Q'_{GaAs-2_0}=Q^+_{AlGaAs} \qquad (32)$$

Q^+_{AlGaAs} is the positive surface charge density ($\frac{\text{coul}}{\text{cm}^2}$) in the AlGaAs composed mostly of uncompensated donor atoms. Q'_{GaAs-2_n} is the surface charge density after irradiation at the nth plane in the GaAs Region and is calculated by appling Guass's law at the nth plane parallel to the interface. Q'_{GaAs-3_n} is the space charge density of the nth segment after irradiation and is calculated from equation 31 using the potential V_n. V_n is the potential at the nth segment relative to the interface and ΔV is the potential difference across the nth segment.

The numerical solution to Poisson's equation is obtained by iteratively choosing $Q_{GaAs-2_0}=-Q^+_{AlGaAs}$ and solving equation 32 until V_n diverges or $E_f-V_n<E_B$. This process is repeated until $Q^+_{AlGaAs}\approx\sum_{n=1}^{\infty}Q_{GaAs-3_n}{}^*\Delta X_n$. ΔV_{th} is then calculation as follows:

$$\Delta V_{th} = \frac{\left[Q^{+\prime}_{AlGaAs} - Q^{+}_{AlGaAs} \right] d_{TOT}}{\varepsilon_{ave}} \tag{33}$$

where the prime indicates the post irradiation value. The calculated Q'_{GaAs-2} due to traps in the GaAs region is plotted versus electron fluence in figure 8 and ΔV_{th} due to ΔQ_{GaAs-2} is plotted in fig. 9 versus electron fluence.

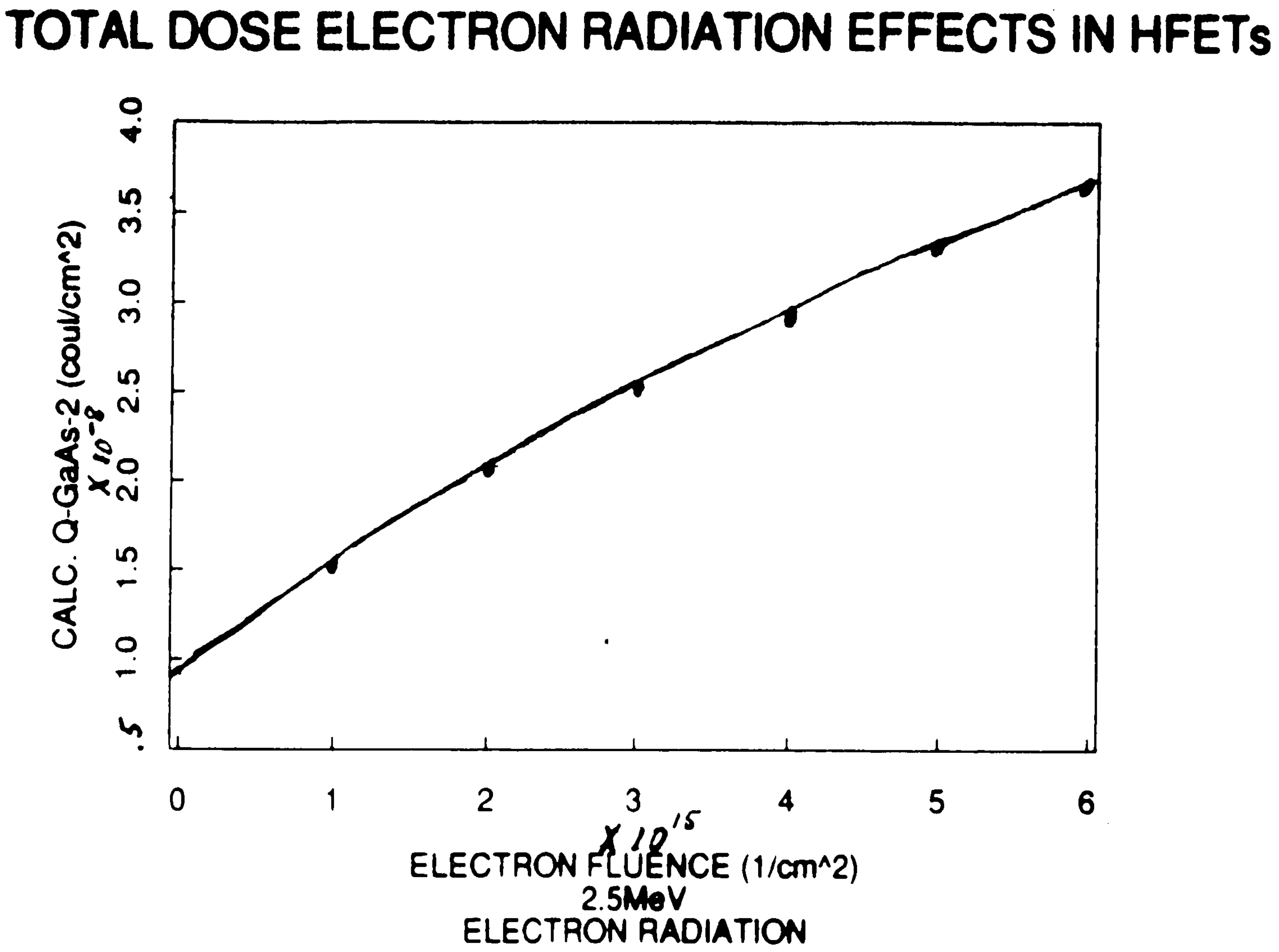

Figure 8. Q'_{GaAs-2} versus electron fluence (Q_{GaAs-2} before irradiation $=8.94X10^{-9}\ \frac{coul}{cm^2}$)

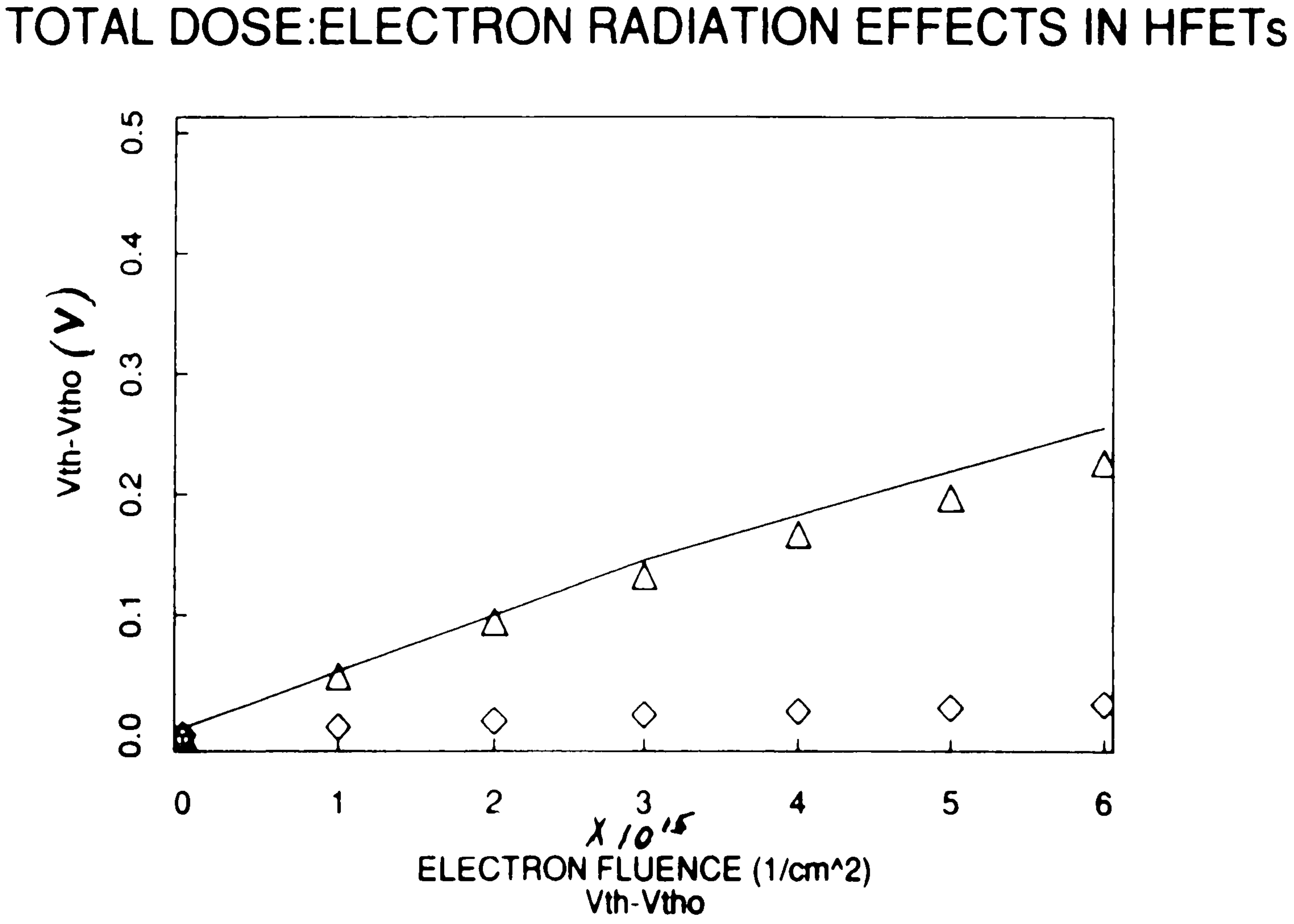

Figure 9. Calculated ΔV_{th} (solid line) versus electron fluence, ϕ. The portion of ΔV_{th} due to the term ΔE_f is represented by the triangles and the portion of ΔV_{th} due to the the term $\frac{\Delta Q_{GaAs} d_{TOT}}{\varepsilon_{ave}}$ is represented by the diamonds.

3.3.3 ΔV_{th} ***Due to*** ΔE_{fi} **It has been shown in section 5.1.2.3 that the radiation induced traps cause Q_{GaAs-2} to increase at threshold. The increase in Q_{GaAs-2} causes the 2DEG charge in the triangular quantum well at the interface to become more confined due to the increased electric field at x=0,**

$F_s=\dfrac{Q_{GaAs-2}}{\varepsilon_{GaAs}}$. From the Hiesenberg uncertainty principle, an increased localization in charge causes an increased spred in energy. The energy levels of the quantized energy states increase with increasing Q_{GaAs-2}. E_{f-th} can be defined as shown in equation 34 by solving for E_f in equation 6 in section 2, considering only the 0th quantized state.

$$E_{f-th}=\frac{k_B T}{q}\ln\left[\exp\left(\frac{q_2 n_{s-th}}{DK_B T}\right)-1\right]+E_o \tag{34}$$

If we assume that n_{s-th} before irradiation is approximately equal to n_{s-th} after irradiation, then $\Delta E_{f-th} \approx \Delta E_{o-th}$. ΔE_{f-th} can be expressed as

$$\Delta E_{f-th} \approx \Delta E_{o-th} \approx \zeta_0\left(\frac{Q'_{GaAs-2}}{q\,\varepsilon_{GaAs}}\right)^{\frac{2}{3}}-\zeta_0\left(\frac{Q_{GaAs-2}}{q\,\varepsilon_{GaAs}}\right)^{\frac{2}{3}} \tag{35}$$

ΔE_{f-th} versus Q'_{GaAs-2} is plotted in figure 10. From figure 8, $\Delta Q_{GaAs-2}=8.9\times10^{-9}\,\dfrac{coul}{cm^2}$ before irradiation and $Q'_{GaAs-2}=3.64\mathrm{X}10^{-8}\,\dfrac{coul}{cm^2}$ for $\phi=6\times10^{15}\,\dfrac{1}{cm^2}$. Figure 10 shows that for this range of Q'_{GaAs-2}, ΔE_f ranges from approximately 0V to .026 V.

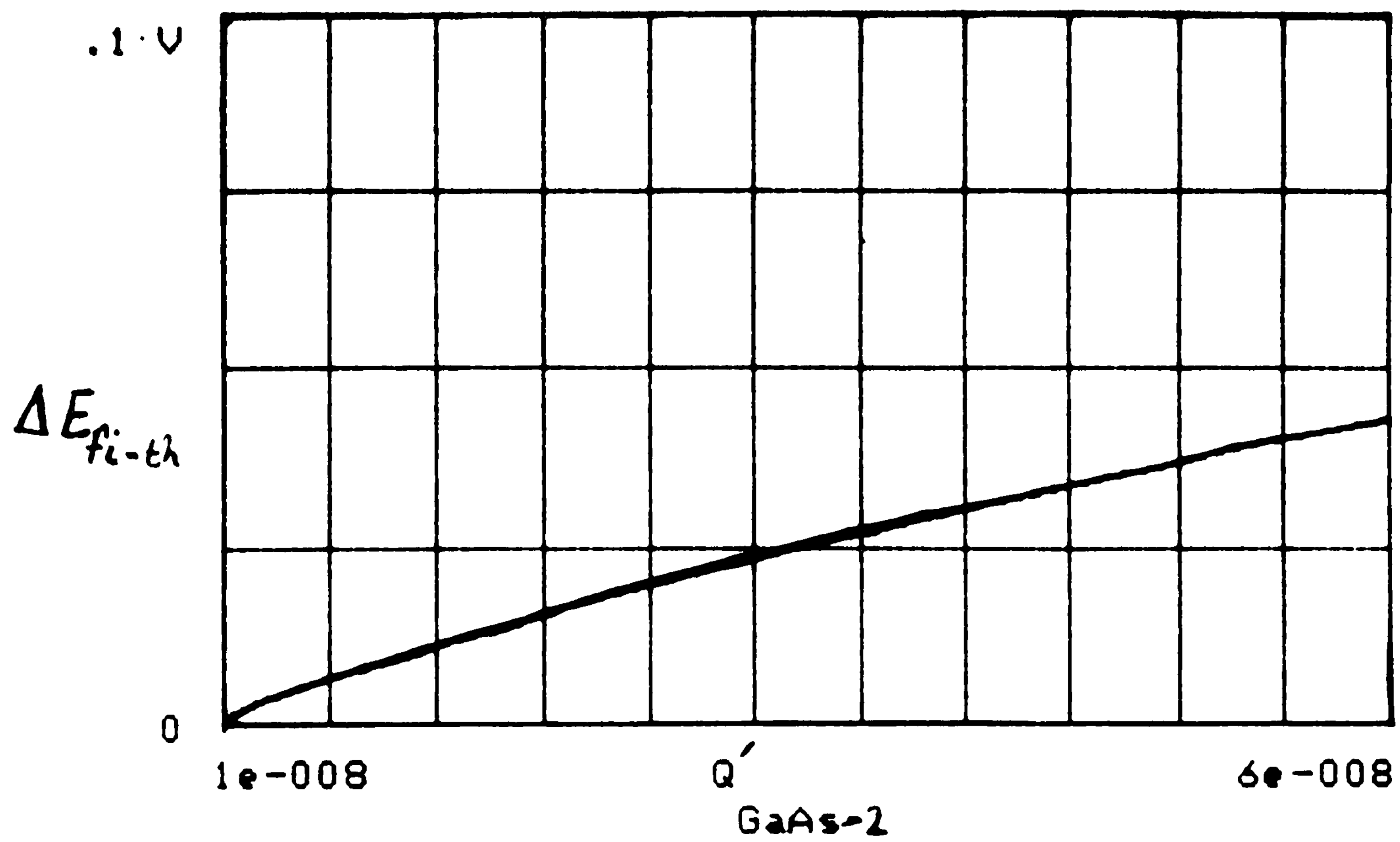

Figure 10. ΔE_{fi-th} at threshold due to an increase in trapped charge in the GaAs region, Q'_{GaAs-2} .

3.3.4 ΔV_{th} *Due to Radiation Induced Traps in the AlGaAs Region:* Traps are also present in the gate to interface region which is approximately 75% AlGaAs. At threshold, this region is depleted and many of the traps are empty and don't change the space charge distribution significantly in the AlGaAs region. Only the electron traps below the Fermi level will be negatively charged and only the hole traps above the Fermi level will be positively charged. An upper limit on ΔV_{th} due to the change in the space charge in the gate to interface region can be calculated by finding the minimum of E_c-E_f. From $(E_c-E_f)_{min}$, an upper limit on the carrier removal rate, R_c, can be found. Since E_c-E_f is larger than $(E_c-E_f)_{min}$ everywhere else in this region, the largest number of traps are filled at w_{min}, and R'_c is the upper limit for the carrier removal rate. The net carrier removal is just $R_c * \phi(\frac{1}{cm^3})$. Once R'_c is found, ΔV_p from equation 26 is calculated using $R'_c * \phi$ as the change in the space charge density throughout the gate to interface region.

The Analysis is simplified by considering the case where only AlGaAs in present between the gate metal and 2-D Gas. The electron and hole trap energy levels in the AlGaAs are approximated as being the same as in GaAs relative to the conduction band and valence band respectively except for the E3 electron trap level which is fixed relative to the valence band.

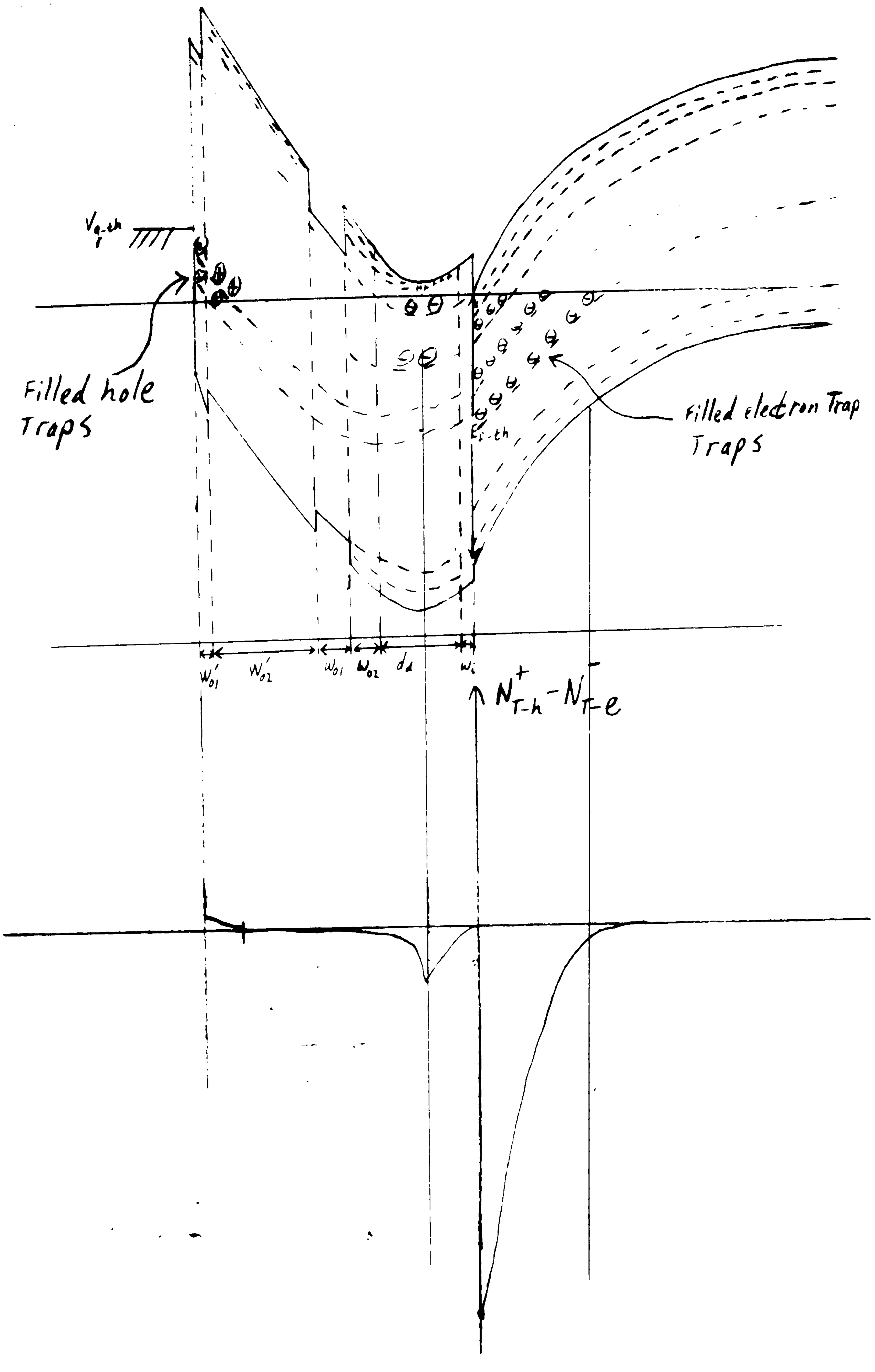

Figure 11. HFET band diagram showing the trap space charge distribution after irradiation. The largest trap space charge density in the AlGaAs occurs at the minimum energy point in the conduction band.

To find $(E_c-E_f)_{min}$, we first assume that the carrier removal rate is the maximum possible value which is just the sum of the electron trap introduction rates, $R_{c-max} \approx 10\frac{1}{cm^2}$. Then after $(E_c-E_f)_{min}$ is found, R_{c-max} is adjusted to a lower value, R'_c, which is still the largest carrier removal rate that occurs at threshold in the gate to interface region. Since the Fermi level is flat in this region, $(E_c-E_f)_{min}$ can be calculated by appling Guass's Law from the interface to the point $w_i+\frac{Q'_{GaAs}}{q\left[N_D-R_{c-max}\phi\right]}$. Equation 36 is the result obtained from appling Quass's Law from the interface to w_{min}. v_2 is the voltage drop from the interface to the minimum energy point, w_{min}, of the conduction band.

$$v_2=\frac{Q_{GaAs}w_i}{\varepsilon_{AlGaAs}}+\frac{Q_{GaAs}{}^2}{q\varepsilon_{AlGaAs}\left[N_D-\phi R_{c-max}\right]}+\frac{2N_DQ_{GaAs}w_i}{\varepsilon_{AlGaAs}\left[N_D-\phi R_{c-max}\right]}-\frac{N_DQ_{GaAs}{}^2}{2q\varepsilon\left[N_D-\phi R_c\right]^2}-\frac{q\phi R_cw_i{}^2}{2\varepsilon_{AlGaAs}} \qquad (36)$$

Using v_2 from equation 36, $(E_c-E_f)_{min}$ can be expressed as $\Delta E_c+E_{f-th}-v_2$. A plot of v_2 versus electron fluence, ϕ, for Q_{GaAs-2} varied from $8x10^{-9}\frac{coul}{cm^2}$ to $6.4x10^{-8}\frac{coul}{cm^2}$ in steps of $8x10^{-9}\frac{coul}{cm^2}$ and $R_c=R_{c-min}$ is shown in figure 12.

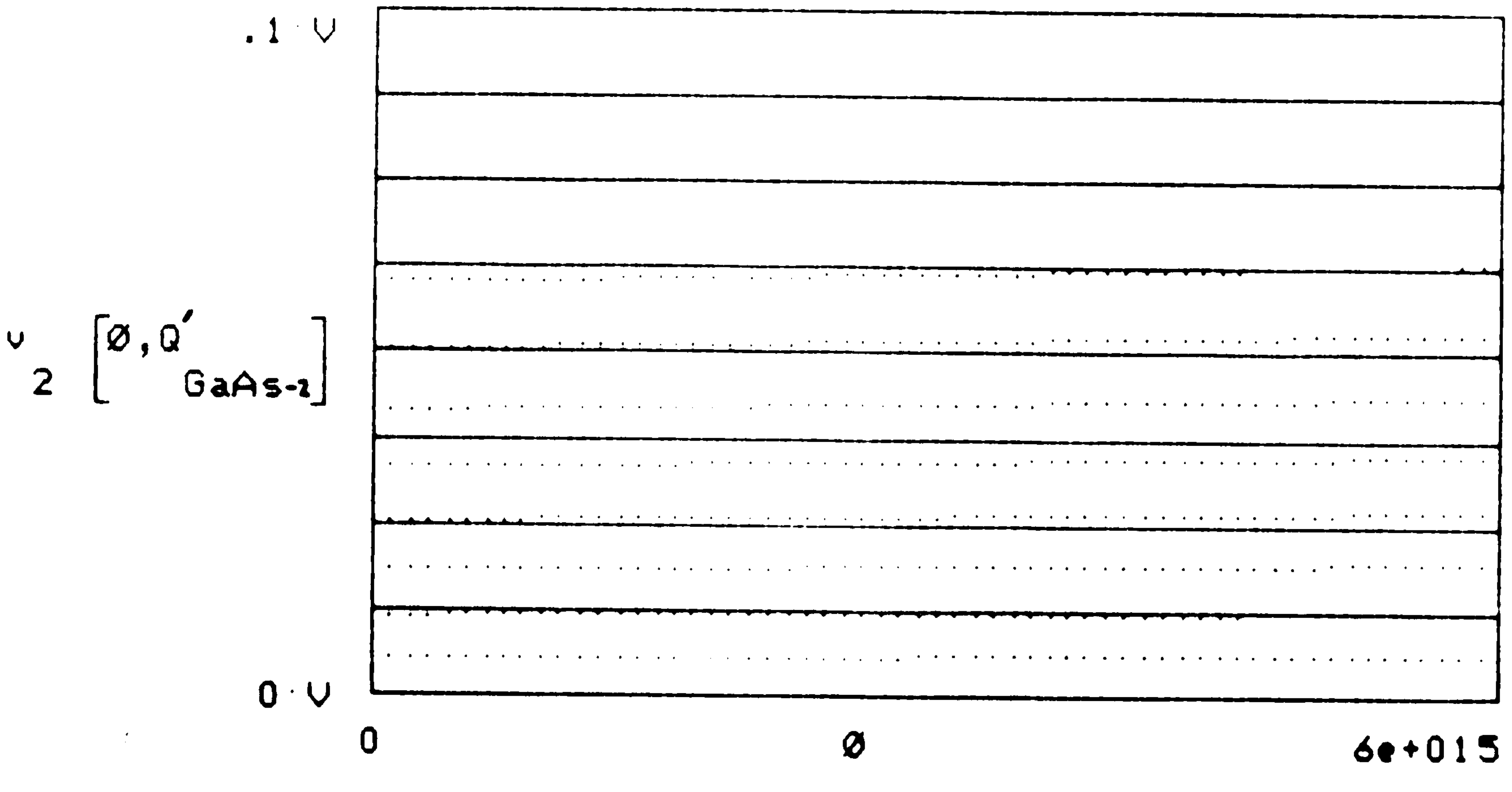

Figure 12. v_2, the potential difference from the AlGaAs/GaAs interface to the minimum potential in the doped AlGaAs at threshold is plotted versus electron fluence for various values of GaAs sheet charge.

Figure 12 shows that using the maximum carrier removal, $10\frac{1}{cm^2} * \phi\frac{1}{cm^2}$, only slightly affects the value

of v_2 and that v_2 depends strongly on Q' From figure 8 , $Q'_{GaAs-2}=3.6x10^{-9}\frac{coul}{cm^2}$, at $\phi=6x10^{15}\frac{1}{cm^2}$, and from fiqure 12 v_2 is approximately .031 V. Therefore $(E_c-E_f)_{min}\geq\Delta E_c+\left[E_g-E_f\right]-v_2\approx.269eV$ in the region between the gate and interface which allows for E_{f-th} to be $\leq E_g$.

Since $E_c-E_{f_{min}}\geq.269eV$ in the AlGaAs region, the minimum carrier removal rate can be adjusted to a lower rate. Figure 13 shows the carrier removal rate as a function of Fermi level where the maximum carrier removal occurs when the Fermi Level is near the conduction band because essentially all the traps are filled. For $E_c-E_f\geq.262eV$, figure 13 shows that $R'_c\leq2\frac{1}{cm^2}$. We use $R'_c=2\frac{1}{cm^2}$ as a uniform carrier removal rate in the region between the gate and AlGaAs/GaAs interface. In the doped AlGaAs region N_D is affectively reduced by $R'_c\phi$ while in the undoped regions the carrier removal is assumed to contribute to a net space charge $R'_c\phi$.

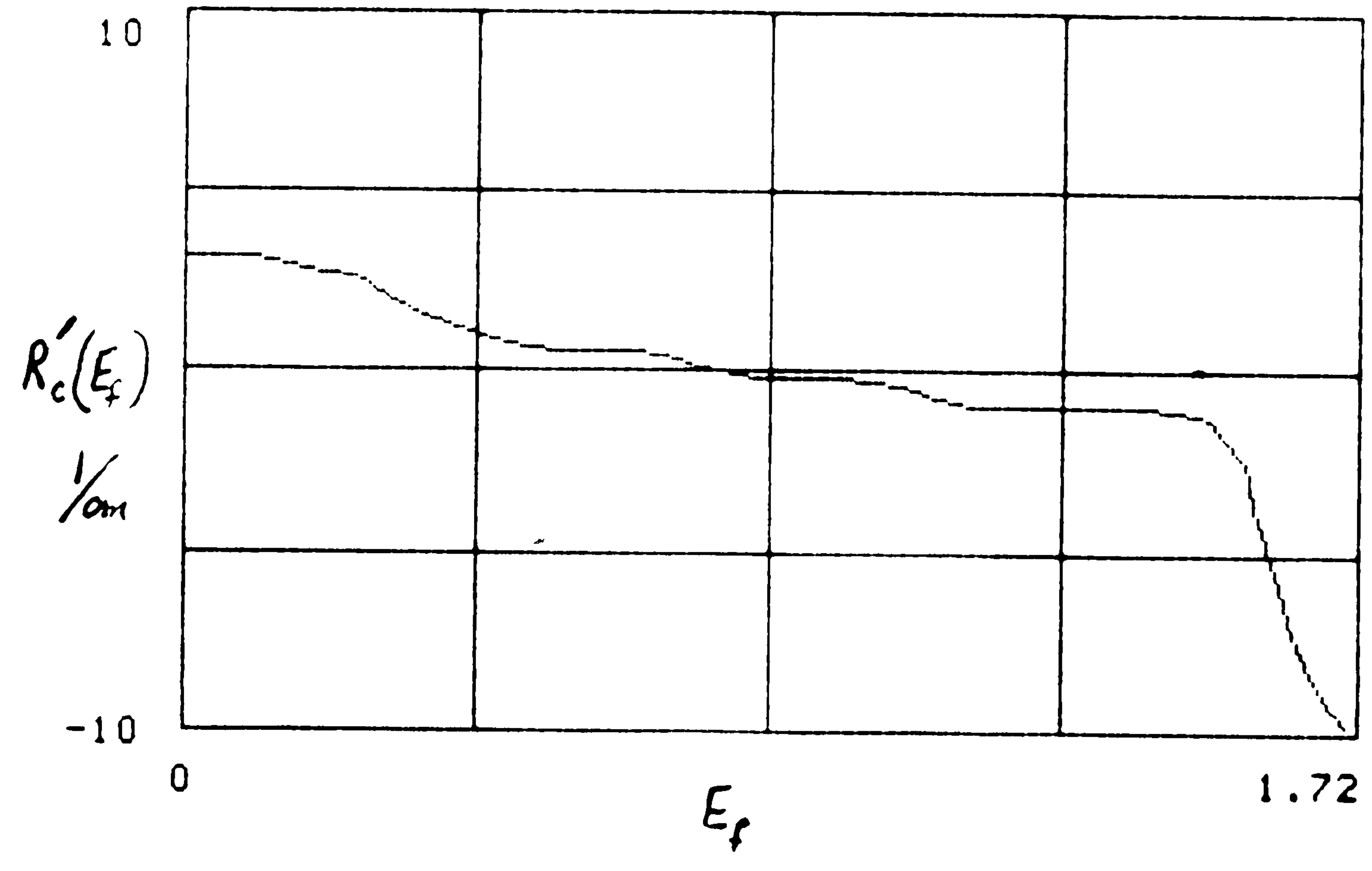

Figure 13. Carrier removal rate versus Fermi Energy.

To find the effect of the adjusted carrier removal, $R'_c=2\frac{1}{cm^2}$, on the threshold voltage, V_p must be recalculated using the new space charge distribution. The change in V_p can be written as:

$$\Delta V_p = \int_0^{gate} \left[\int_0^{x} \frac{\Delta Q(x')}{\varepsilon_{ave}} dx' \right] dx \tag{37}$$

where ΔQ is the change in the space charge distribution after irradiation in the gate to interface region. The integration yields:

$$\Delta V_{p-max} = \frac{qR'_c \phi d_{TOT}^2}{2\varepsilon_{ave}} \tag{38}$$

For $R_c = 2\frac{1}{cm}$ and $\phi = 6x10^{15}\frac{1}{cm^2}$, $\Delta V_{p-max} = .044V$ and $\Delta V_{th} \ll .044V$ from charged traps in the gate to interface region. This worst case analysis shows that the depletion region contributes only slightly to the threshold voltage shifts for electron fluences $\leq 6x10^{15}\frac{1}{cm^2}$.

4. EXPERIMENT

4.1 Experimental Procedure

Heterojunction FETs manufactured by AT&T were irradiated without bias with 2.5MeV electrons. The 2.5MeV electron energy was used because it's well above the experimentally determined energy threshold for causing permanent damage in GaAs, ≈.6MeV and because the Van de Graaff accelerator was stable at 2.5MeV. Eight depletion mode HFETs were used in the study. Approximately fifteen minutes after each radiation exposure, the devices were DC Characterized. The characterization consisted of the following measurements :

1. I_{ds} VS V_{ds}.
2. I_{ds} VS V_{gs}.
3. I_{gs} VS V_{gs}.

The voltage ranges and steps are summarized in Table 3.

TABLE 3: DEVICE CHARACTERIZATION SUMMARY

TEST	RANGE		STEPS	
	V_{gs}	V_{ds}	V_{gs}	V_{ds}
I_{ds} VS V_{ds}	-.4V to .7V	0V to 2V	.1V	.05V
I_{ds} VS V_{gs}	-1V to .7V	.02V to 1.4V	.01V	.2V,.5V,.8V,1.1V,1.4V
I_{gs} VS V_{gs}	-1.8V to .3V	---	---	---

Transconductance curves were obtained from the derivative of the I_{ds} VS V_{gs} curves. After DC characterization, the devices are once again irradiated. The radiation induced damage is accumulated over each exposure.

4.2 Test Set-up/Van de Graaff Accelerator

The devices used in the experiment were mounted in ten lead packages with four HFETs per package. One package per radiation exposure was mounted on a metal plate which is aligned in front of the Van de Graaff electron beam. The package mounting fixture, shown in figure 14, has a front and back plate. The front plate, the metal plate closest to the beam, has a .564 cm diameter aperture. The front plate is too thick for electrons to penetrate and is grounded allowing electrons only through the aperture area to be incident on the DUT. The second plate, which has the package mounted on it, is connected through a current meter to ground. The package, mounted on the second plate, is aligned directly behind the aperture in the front plate. The electrons that pass through the aperture are incident on the DUT and collected by the second plate. The electrons collected by the second metal plate are measured by the current meter. Since the separation between the front plate and back plate is small, ≈2cm, the beam dispersion as small. Therefore electron current density incident on the device is approximately equal to the electron current density leaving the front plate aperture. The electron fluence ($\frac{\text{electrons}}{\text{cm}^2}$) for each exposure can be calculated by integrating the current collected by the second plate and dividing by the aperture area of the first plate. The electron fluence can be expressed as:

$$\phi=\frac{1}{\pi\,(.56\mathrm{cm})^2}\int_0^T I_{collected}\,dt. \qquad (24)$$

4.3 HFET Geometry And Processing

A cross-sectional view of the HFET structure is shown in figure 3. The gate contact is made with WSi_x on a [redacted]A undoped GaAs layer. Underneath the undoped GaAs layer is a [redacted]A undoped AlGaAs layer. These two layers provide the additional gate to 2DEG spacing required for DFET operation while providing an etch stop during an Aluminum etching process step, which is used to etch the undoped AlGaAs layer away to create an EFET structure. Following the undoped AlGaAs is a [redacted]A undoped GaAs layer, a [redacted]A undoped AlGaAs layer and then a [redacted]A n^+AlGaAs. An undoped AlGaAs spacer layer follows, to shield the AlGaAs/GaAs interface from the diffusion of impurities from the doped AlGaAs layer. A [redacted]um undoped GaAs layer follows, and is grow on semi-insulating substrate.

The 2DEG is formed at the interface of the GaAs-AlGaAs layer. The depletion and enhancement mode HFETs are formed using a self-aligned refractory gate technology. In this technology, the source and drain contacts are made after the WSi_x gate contact is deposited. The source and drain contacts are ion implanted on both sides of the gate by using the gate metal as a refracting shield.

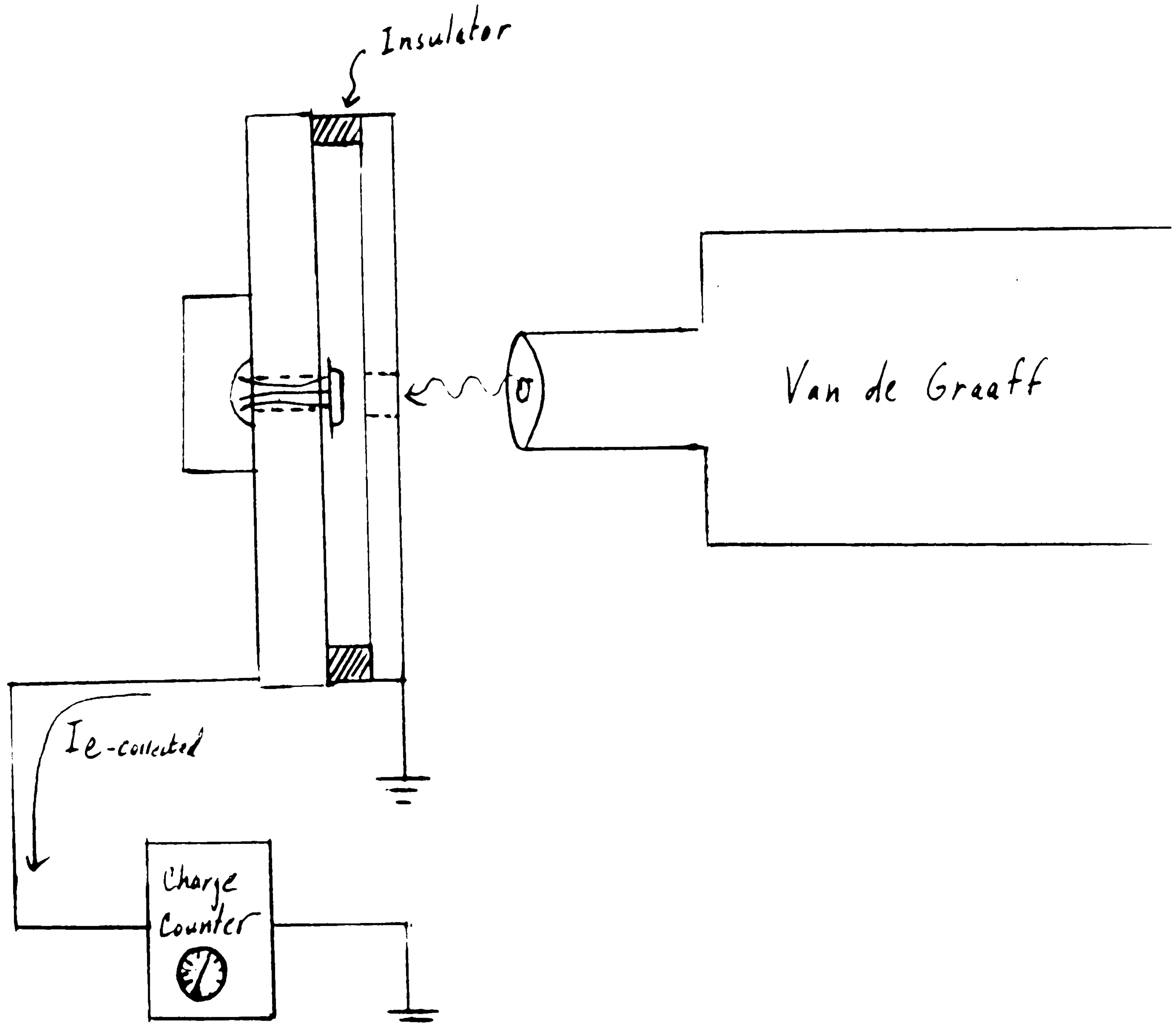

Figure 14. Test set-up for irradiating HFETs

5. EXPERIMENTAL RESULTS AND ANALYSIS

5.1 Changes in Threshold Voltage

Figure 15-a and 15-b shows the I_{ds} versus V_{gs} curves for two different HFETs before and after being irradiated with 2.5MeV electrons. In all cases the threshold voltage has shifted in the positive direction. The threshold voltage is determined by extrapolating the linear part of the I_{ds} versus V_{gs} curve to the Ids=0 line.

In figure 16 the measured ΔV_{th} for the D-HFETs is plotted versus fluence (*). The calculated threshold from section 3.3 is also shown in figure 16 (solid line). The calculated curves compare well to the experimental data except at the high end of the fluence levels used in the experiment. From the calculations made in section 3.3, ΔV_{th} is dominated by the accumulation of charge in the GaAs region and by the increase in energy of the quantized energy levels at the GaAs-AlGaAs interface.

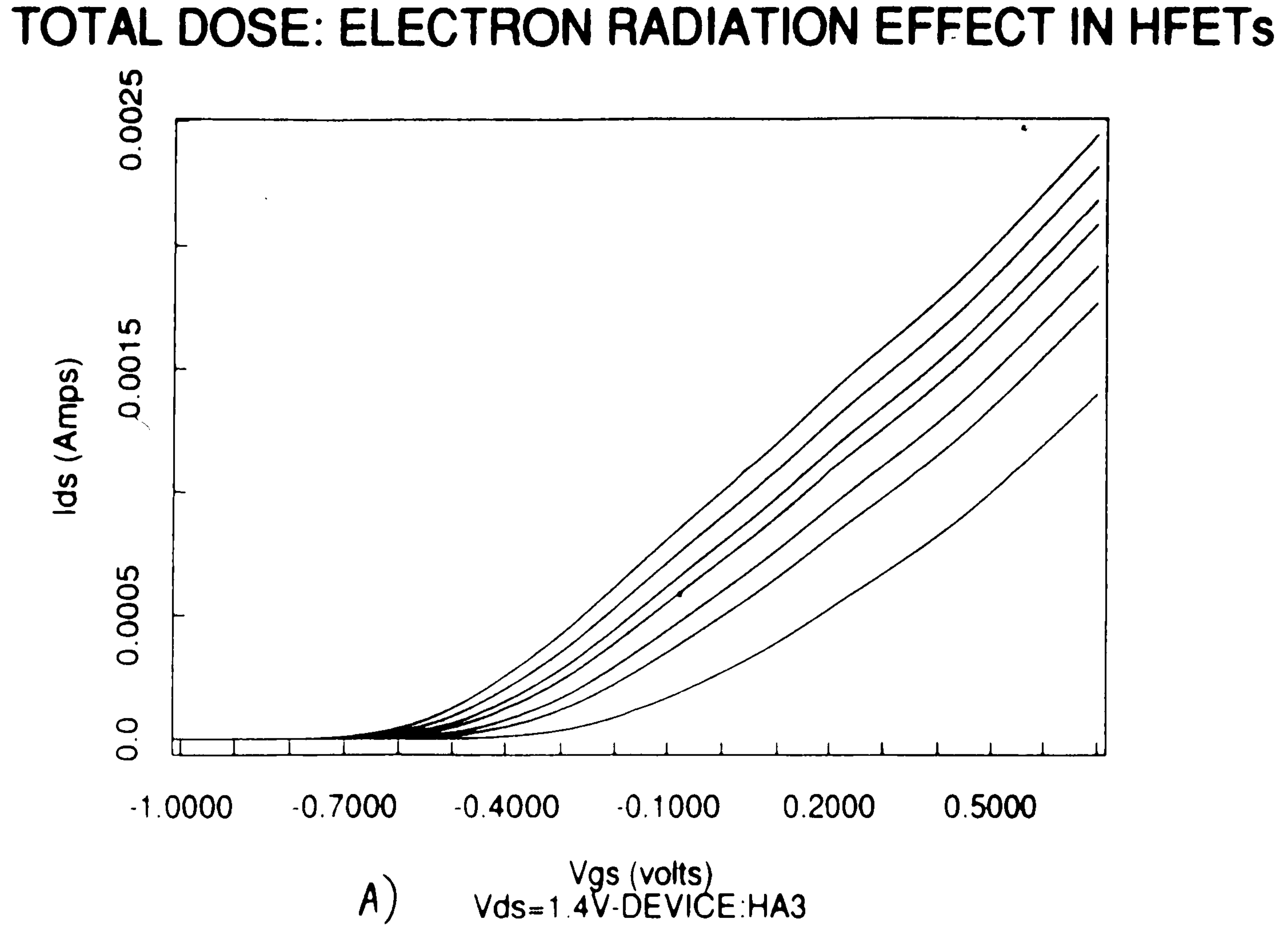

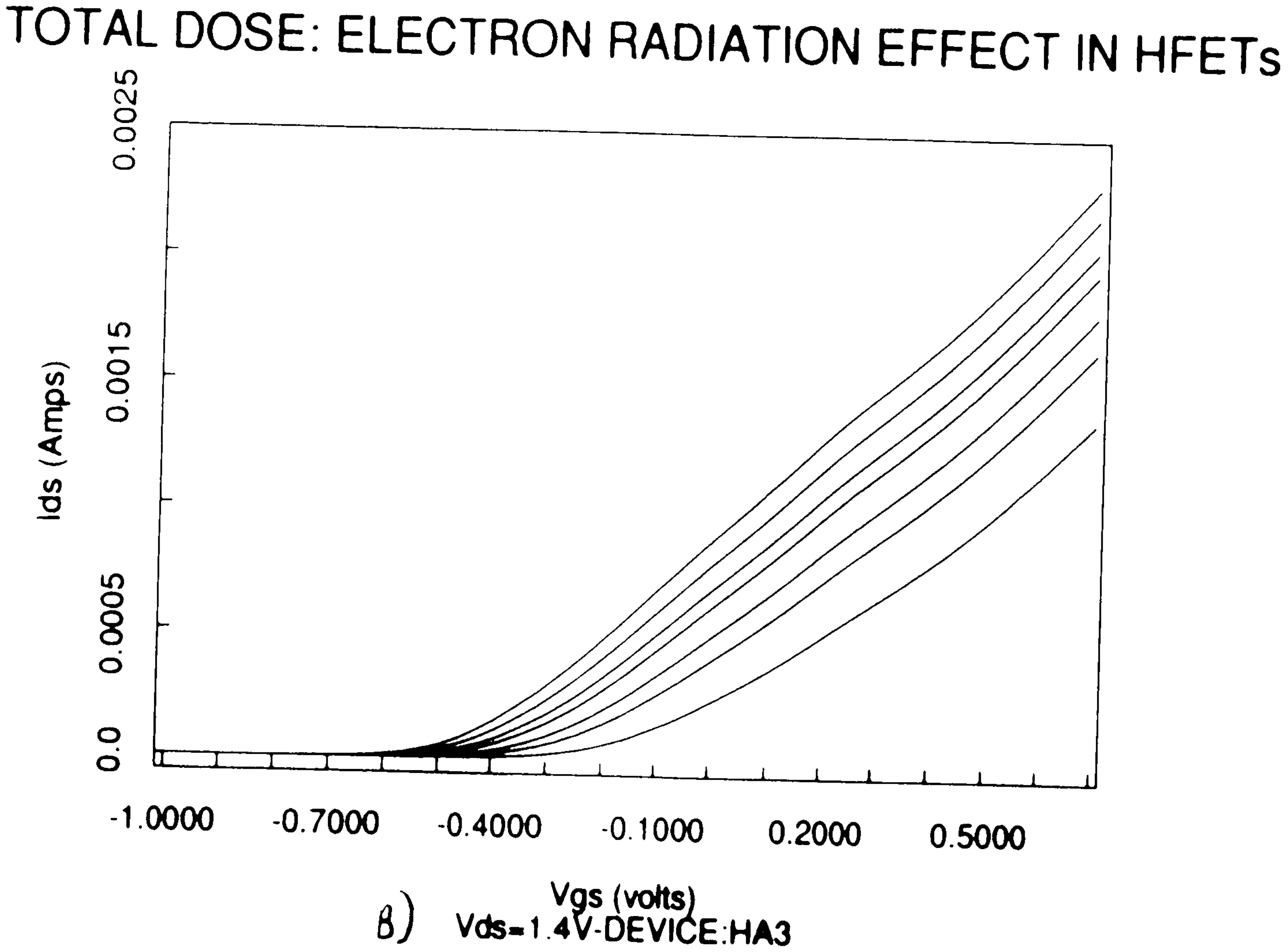

Figure 15. I_{ds} versus V_{gs} for two AT&T D-HFETs before and after irradiation with 2.5 MeV electrons (Electron Fluence=ϕ=0,6.75X10^{14},1.4X10^{15},3X10^{15},4X10^{15},6X10^{15} 1/cm^2).

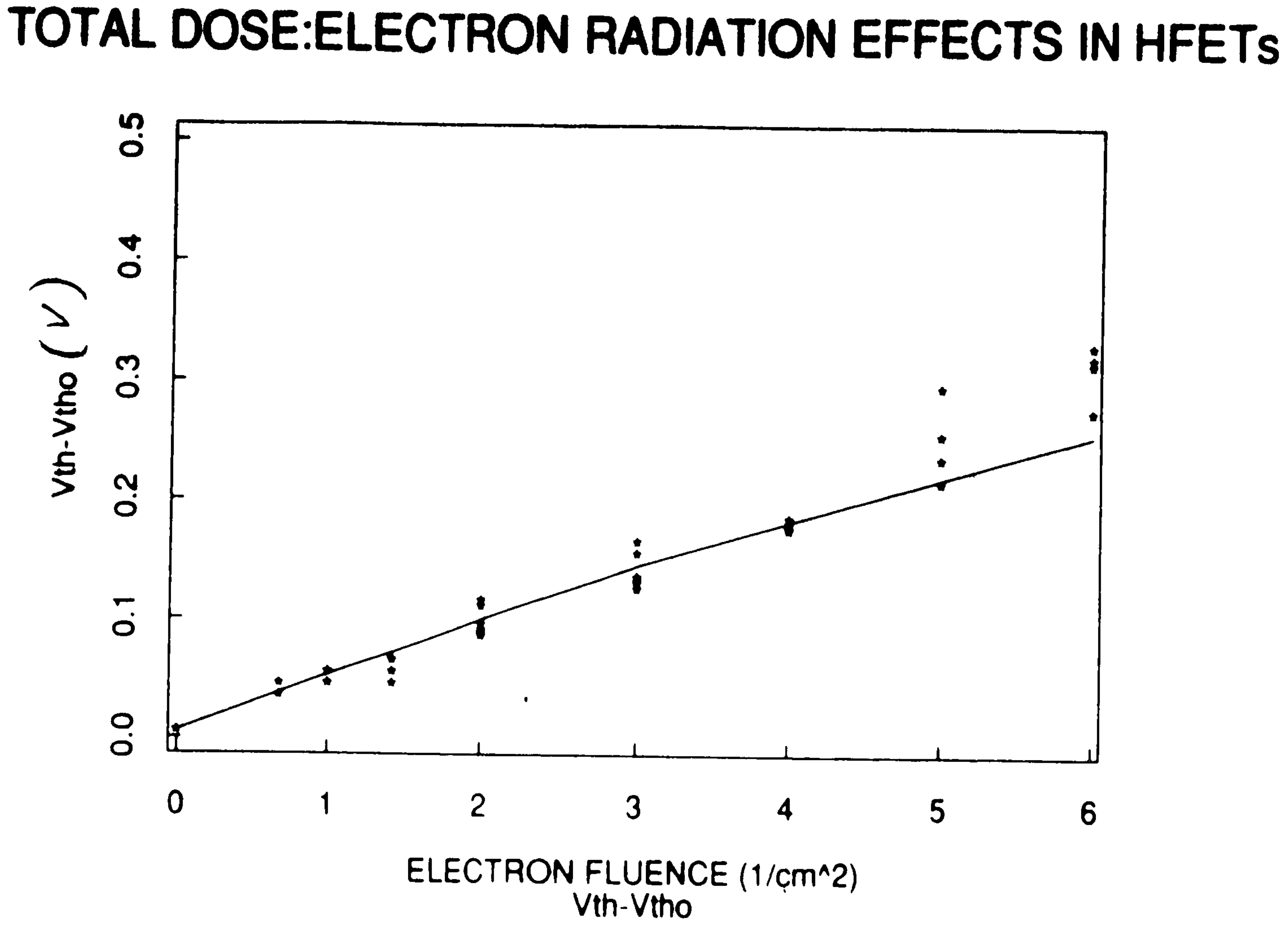

Figure 16. Comparison of calculated ΔV_{th} from section 3.3 (solid line) and measured ΔV_{th} (*).

5.2 Changes in Transconductance Characteristics

The transconductance, $\frac{dI_{ds}}{dV_{gs}}$ before an after irradiation for two depletion mode HFETs is shown in figure 17 for $-1.0V \leq V_{gs} \leq .7V$ and $V_{ds}=1.4V$.

The curves saturate,then decrease slightly before increasing again beyond the first saturation maximum. The first saturation in the transconductance occurs when the 2-D gas electron concentration approaches η_{so}. η_{so} is the maximum 2-D gas sheet charge and occurs when that AlGaAs-GaAs heterojunction is in thermal equilibrium without interaction with the electric fields from the gate bias. As Vg becomes more positive, the 2D-gas saturates, and the N^+ AlGaAs layer starts to become undepleted and conduct . Since the AlGaAs has a lower mobility, and saturation velocity, $G_m=\frac{dI_{ds}}{dV_{gs}}$ continues to decrease but then the parasitic quantum starts to fill as V_{gs} becomes more positive. At this point G_m increases beyond the first saturation peak, since the parasitic quantum well is closer to the gate than is the 2-D Gas.

This transconductance characteristic has been simulated using the AT&T "SIGMA" program by J. Lentz et al from AT&T. This software program runs on the Sun Workstation and solves Poisson's Equation and Schrodinger's Equation simultaneously in one dimension for HFET structures. Figure 18 shows

n_{s-TOT} versus V_g where n_{s-TOT} is the net conduction band surface electron density in the device. This includes the 2DEG, parasitic AlGaAs channel, and parasitic quantum wells.

After being irradiated, the transconductance curves shifted in the positive Vgs direction as would be expected since the threshold voltage also shifted in the positive Vgs direction. The first saturation in the transconductance curve occurs at a lower G_m value. The dip in the transconductance also decreases with increased electron fluence. At a fluence level of $6X10^{15}$ $\frac{\text{electrons}}{\text{cm}^2}$ the dip has completely disappeared. The reduction in the first saturation peak is caused by a decrease in $\frac{d\eta_s}{dV_{gs}}$ due to the loss of conduction band electron to traps near the GaAs interface and from a decrease in the saturation velocity from impurity scattering. The decrease in the dip after each irradiation is believed to be caused by the increase in the net negative charge at the GaAs interface. This additional negative charge, which increases V_{th} also causes the 2DEG to saturate at a higher gate voltage. As the gate voltage at which the 2-D gas saturates approaches the threshold voltage of the parasitic quantum well, the parasitic quantum well starts to conduct before the 2DEG is totally saturated. When this occurs, G_m no longer decreases. In figure 19, the band diagrams at the AlGaAs/GaAs interface are draw with and without traps in the GaAs and AlGaAs for $V_{gs}=V_{2-D-sat}$, where $V_{2-D-sat}$ is the gate voltage at which the 2DEG saturates. The depletion region width in the N^+ AlGaAs region measured from the point in the AlGaAs region where the electric field is zero to the AlGaAs-GaAs interface, is larger when the traps are present in the GaAs. Also the parasitic quantum well conduction band edge is closer to the Fermi-level. As V_{gs} is increased the parasitic quantum well becomes occupied and starts to conduct.

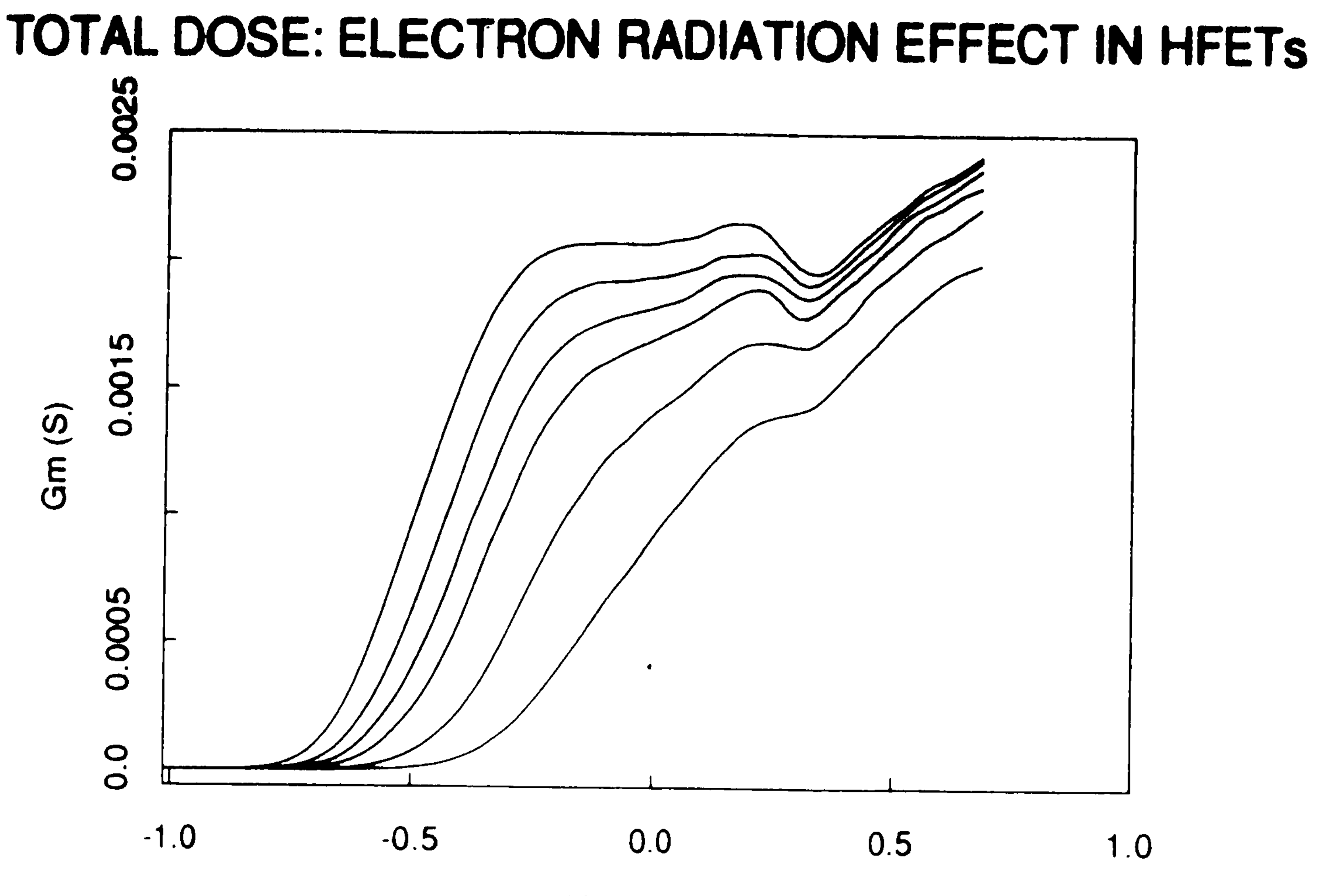

TOTAL DOSE: ELECTRON RADIATION EFFECT IN HFETs

TRANSCONDUCTANCE(Vds=1.4V)-DEVICE:HC3

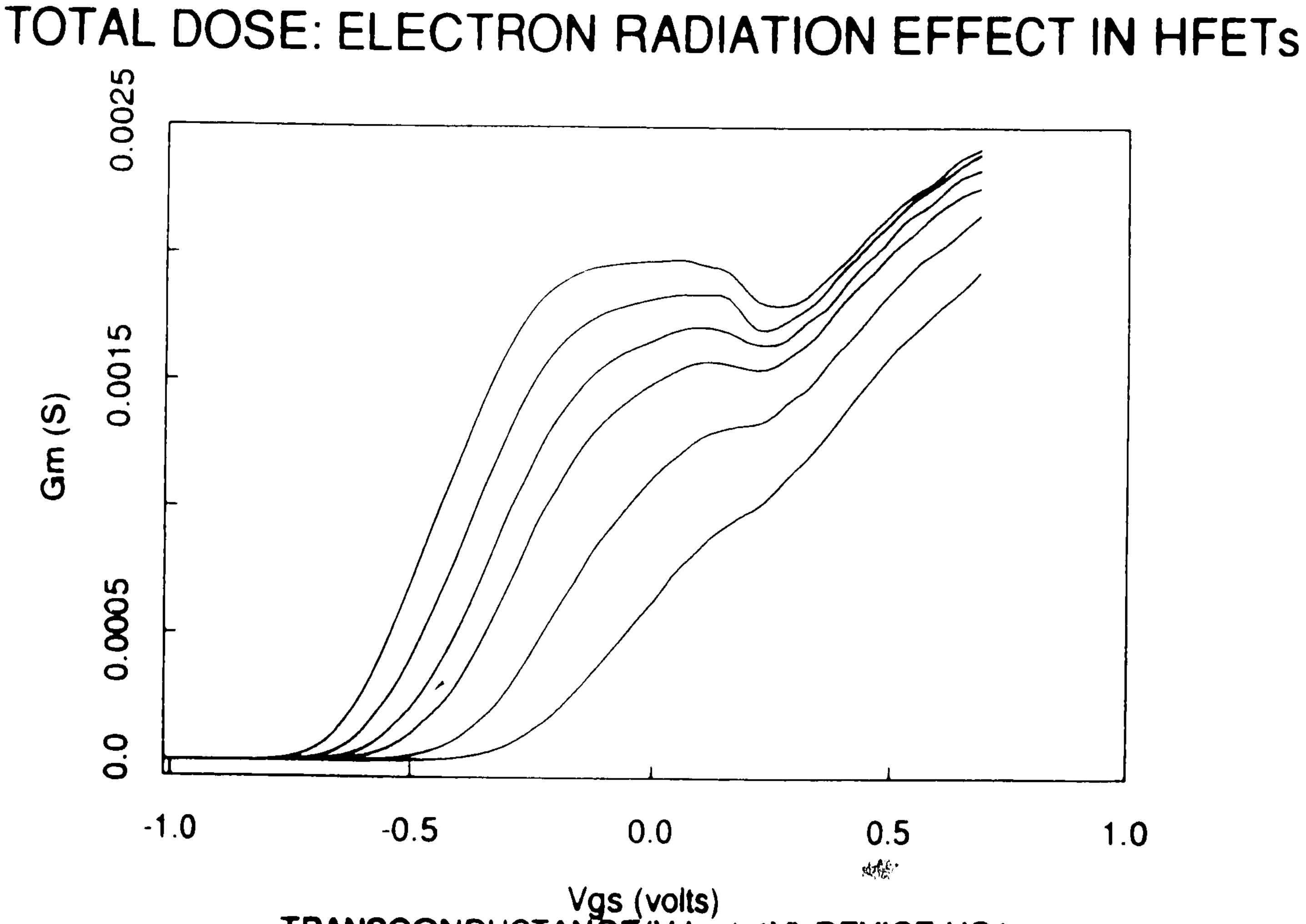

TOTAL DOSE: ELECTRON RADIATION EFFECT IN HFETs

TRANSCONDUCTANCE(Vds=1.4V)-DEVICE:HC4

Figure 17. Transconductance versus V_g before and after irradiation (Electron Fluence = ϕ=0, $1X10^{15}$, $2X10^{15}$, $3X10^{15}$, $5X10^{15}$, $8X10^{15}$ $\frac{1}{cm^2}$).

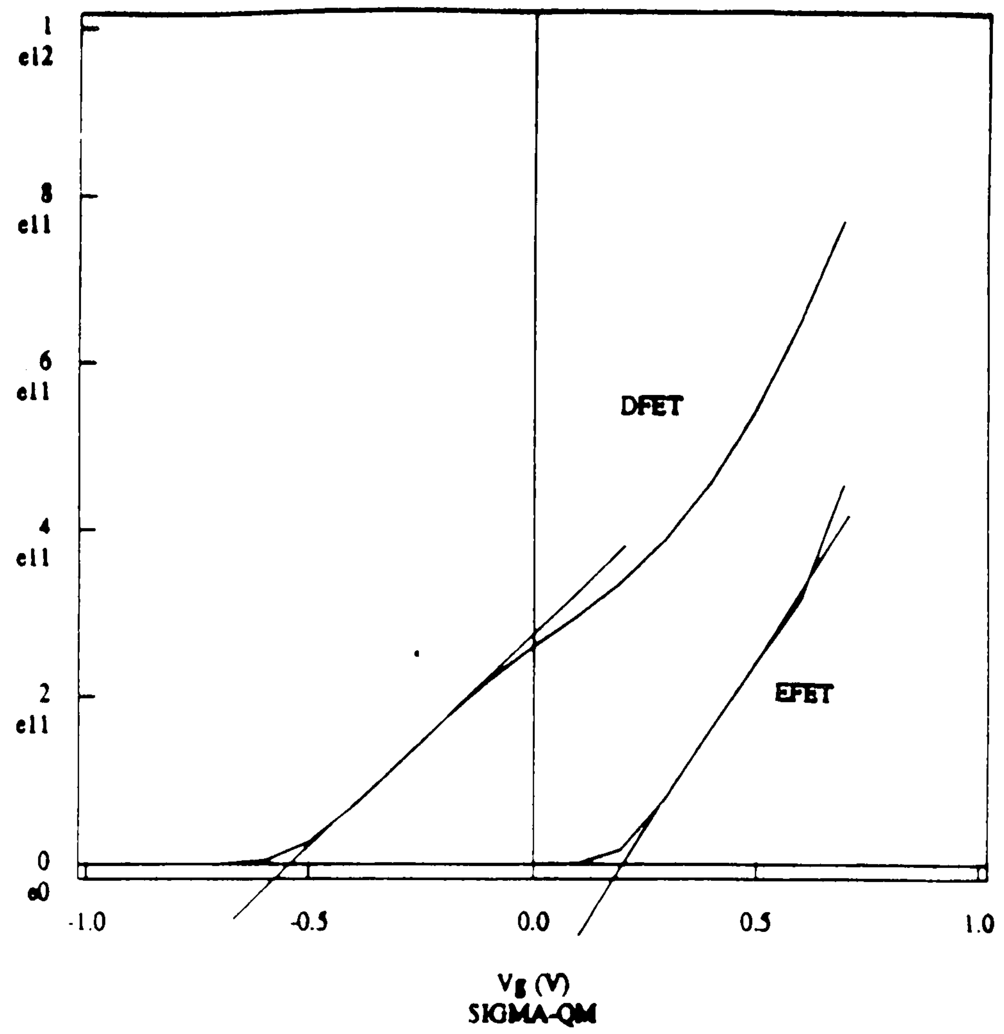

Figure 18. Numerical calculation of the total surface charge density in AT&T D-HFET (including 2-D gas, parasitic AlGaAs channel, and parasitic quantum well) as a function of V_{gs} .

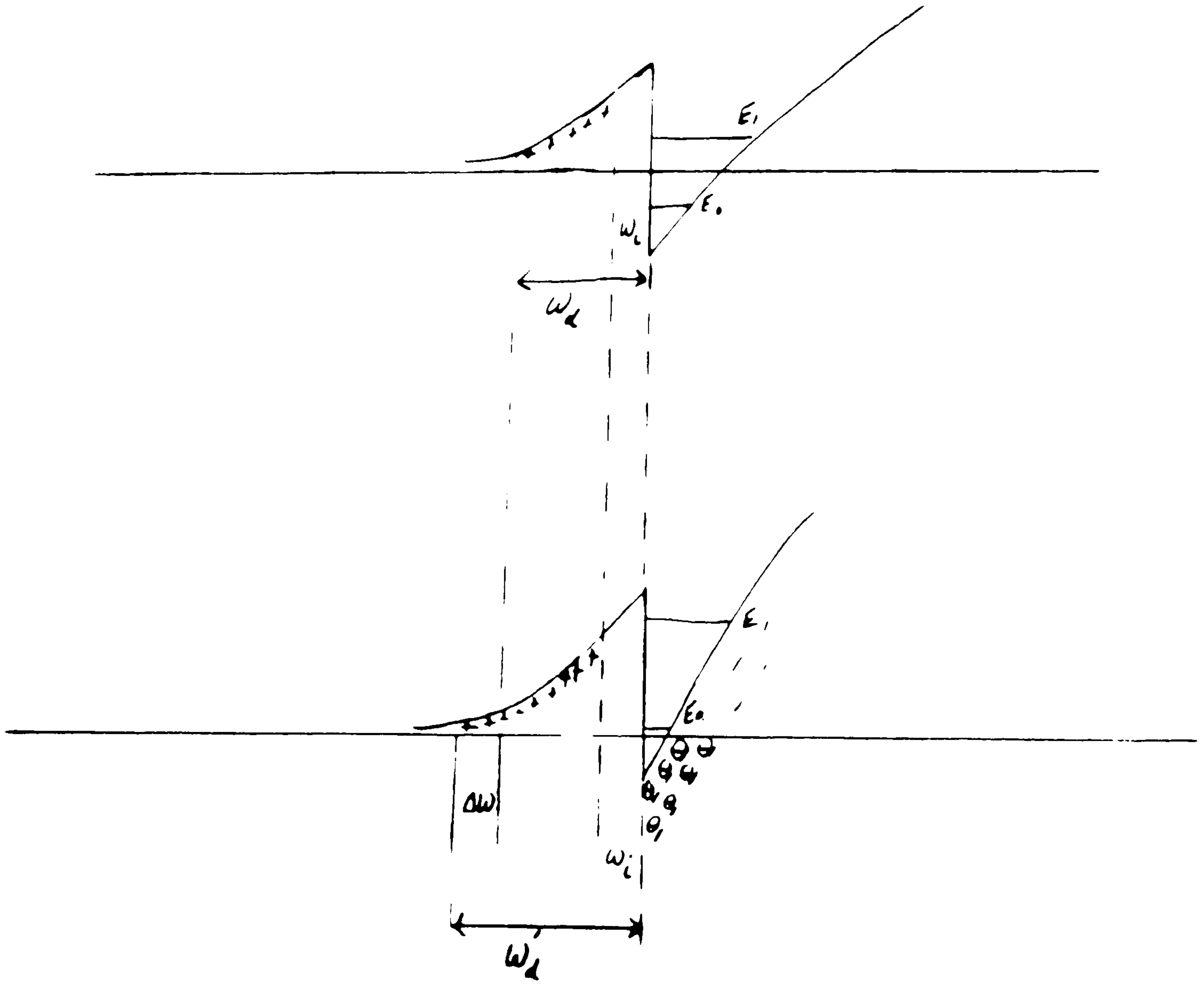

Figure 19. Band bending at the AlGaAs/GaAs interface at $V_g=V_{2D-on}$ before and after irradiation.

5.3 Changes in Drain Saturation Current

The degradation of the drain current with increasing irradiation dose has been evaluated. Figure 20-A shows the change in the I_{ds} versus V_{ds} curve for $V_{gs}=0V$. The zero gate voltage condition is a particularly important curve to evaluate since the D-HFETs are most commonly used as a resistive component in inverter circuits with the gate and source nodes connected together. A large percent of the change in drain saturation current can be contributed to ΔV_{th}. A comparison between I'_s and $I_{so}(V_g-\Delta V_{th-meas})$ is made in figure 20-B. I'_s is the drain saturation current at $V_{ds}=1.4V$ and $V_{gs}=0V$ after irradiation and $I_{so}(V_g-\Delta V_{th-meas})$ represents the drain saturation current reduced by the effects of ΔV_{th} only, where ΔV_{th} is a function of ϕ. Figure 20-B shows that ΔV_{th} contributes to more than 80% of ΔI_{ds}. Therefore the change in the saturation velocity and the additional charge trapping for $V_g>V_{th}$ contributes a combined effect of <20% at high level of electron fluence $\approx 6X10^{15}\frac{1}{cm^2}$. The ratio of $\frac{\Delta I_{so}(V_g-\Delta V_{th})}{\Delta I'_s}$ is much smaller at lower electron fluence levels. The change in the saturation velocity maybe a more dominant component of ΔI_{ds} at $\phi<1X10^{15}\frac{1}{cm^2}$.

Figure 21 shows the degradation in $\frac{I_{ds}}{I_{dso}}$ for $V_{gs}=0V$ and $V_{ds}=1.4V$. I_{dso} is the drain current before irradiation. A linear fix to the data in figure 21 yields:

$$\frac{I_{ds}}{I_{dso}}=1.0-1.15X10^{-16}\ \Phi \tag{39}$$

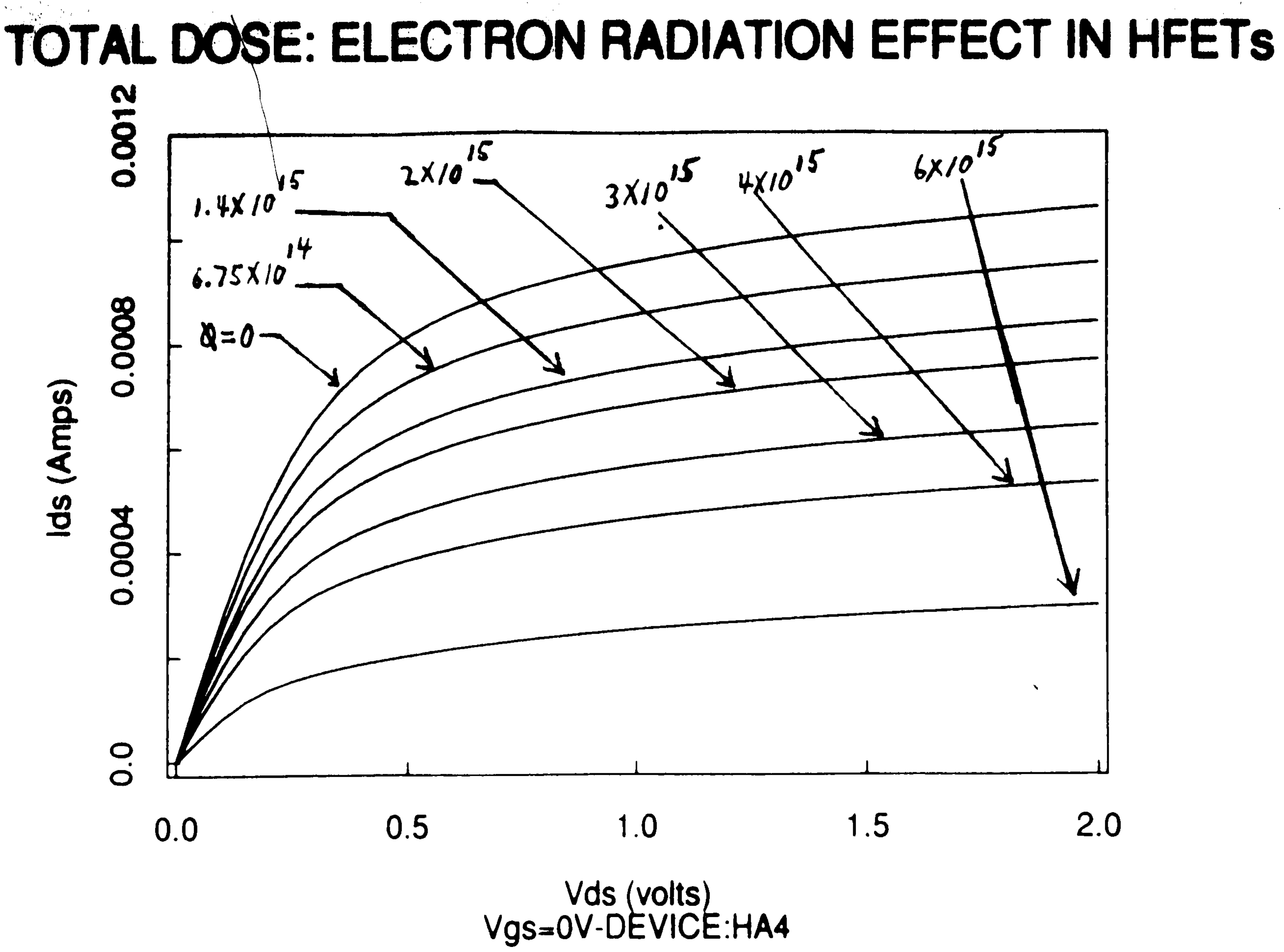
TOTAL DOSE: ELECTRON RADIATION EFFECT IN HFETs

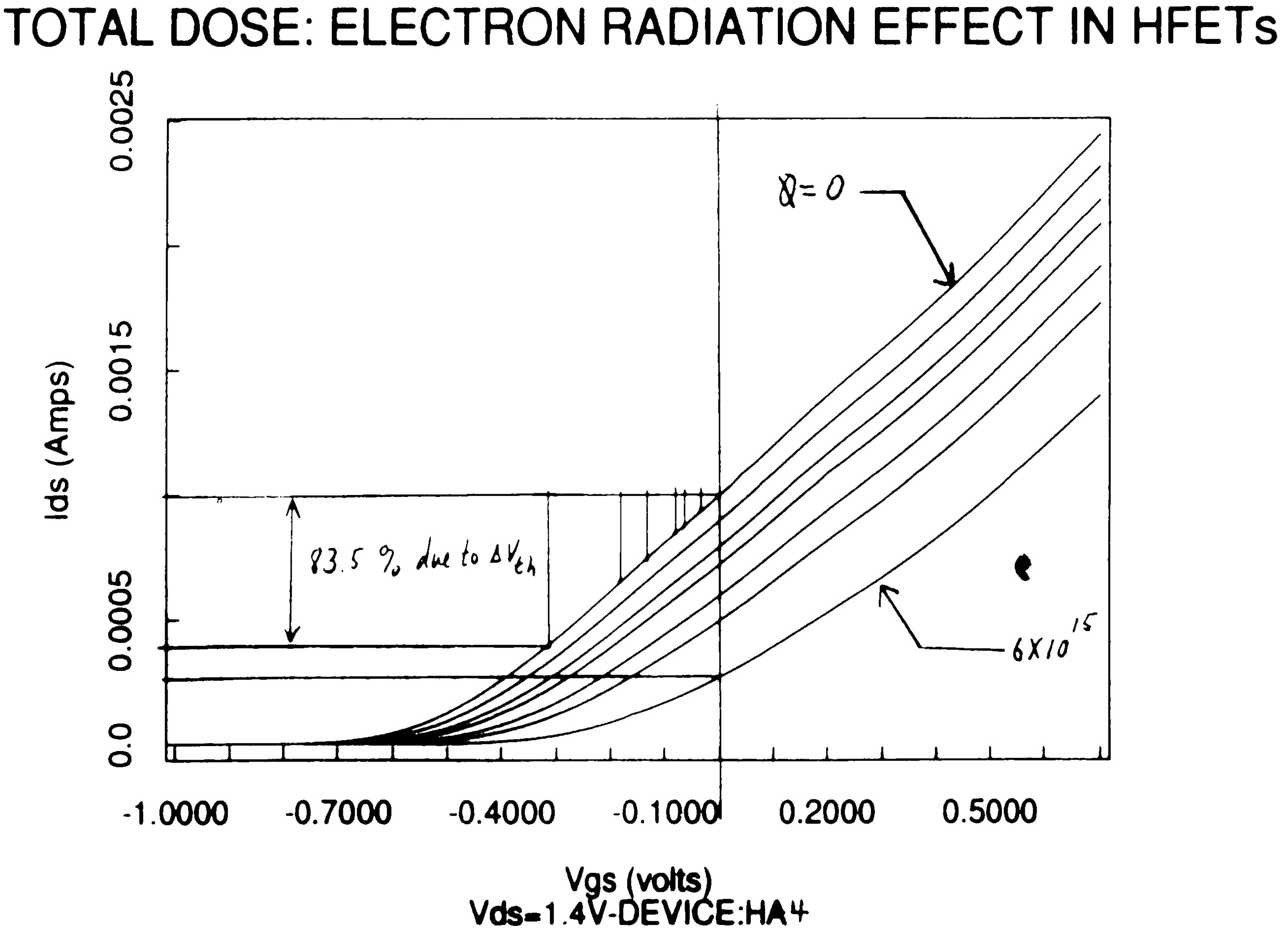
TOTAL DOSE: ELECTRON RADIATION EFFECT IN HFETs

Figure 20. A: I_{ds} versus V_{ds}, B: I_{ds} versus V_{gs} before & after irradiation (V_{gs}=0V, Electron Fluence=ϕ=6.75X10^{14}, 1.4X1015, 2X10^{15}, 3X10^{15}, 4X10^{15} , 6X10^{15} $\frac{1}{cm^2}$).

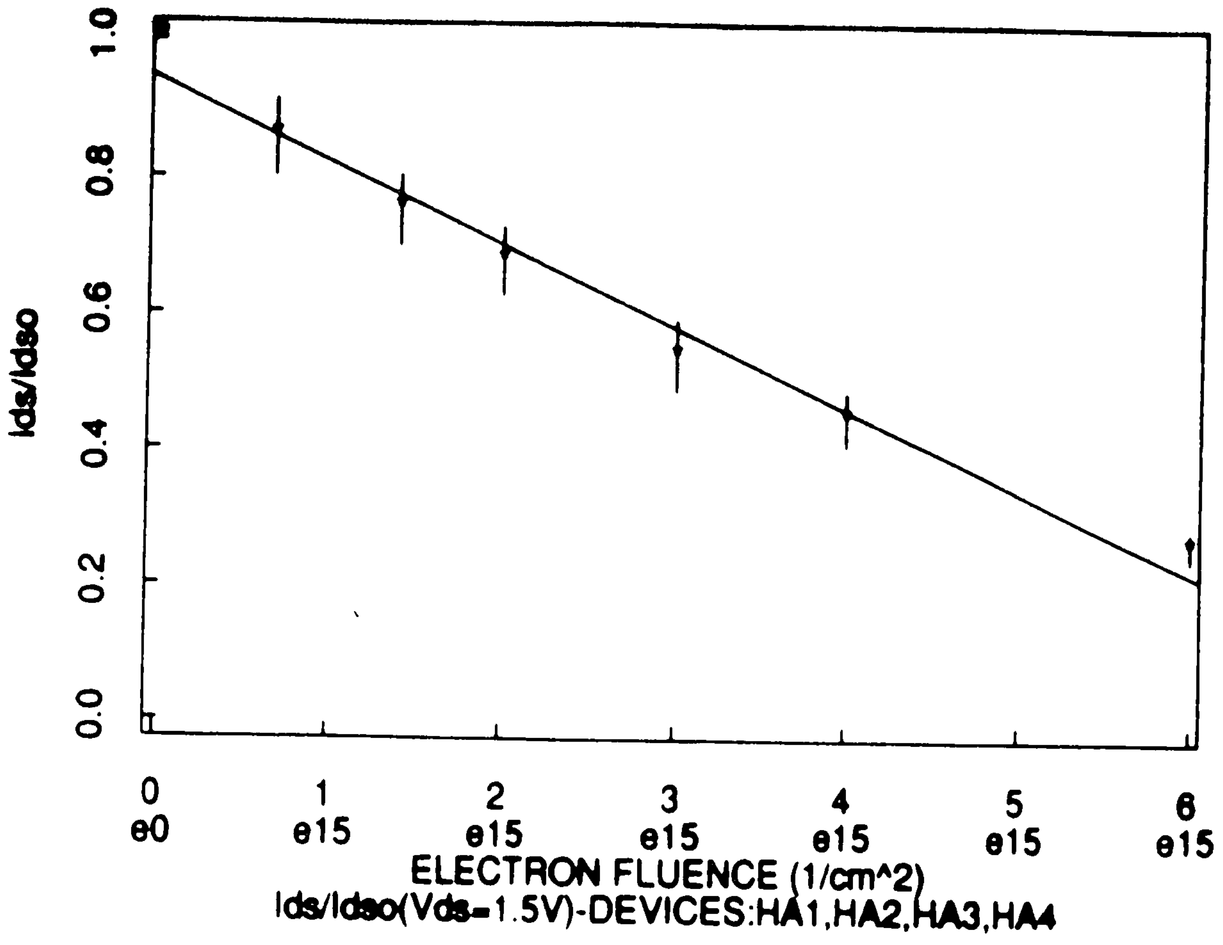

Figure 21. $\frac{I_{ds}}{I_{dso}}$ versus electron fluence, ϕ.

5.4 Changes in Reverse Bias Gate Current Characteristics

The reverse bias HFET gate current characteristics, are shown in figure 22 for several HFETs used in this study. The solid line curve represents I_{gs} versus V_{gs} before being irradiated and the dotted line after $6x10^{15}\ \frac{\text{electrons}}{\text{cm}^2}$ of 2.5 MeV electron irradiation. In general the changes are not vary significant. In all cases, the reverse bias gates current increased with irradiation dose. The change in reverse gate current seems to be proportional to the pre-irradiation value. For example, the reverse gate current in device HA3 was less than -.1 nA at V_{gs}=−1.8V before irradiation and changed by only about -15 pA after $6x10^{15}\ \frac{\text{electrons}}{\text{cm}^2}$. Device HA4 had a large reverse gate current of about -.5nA before being irradiated. After $6x10^{15}\ \frac{\text{electrons}}{\text{cm}^2}$, the gate current in device HA4 increased by about -250 pA.

An increase in reverse gate current with radiation, is what would be expected due to the increase in generation current in the depletion region of the gate Schottky barrier. In the depletion region of a reverse biased junction, the recombination rate is zero since the free carrier density p and n are neglectable and a net generation of electron hole pairs take place. It is also believed that surface states are created at the surface between the gate and source, which increase the reverse gate currents due to a conductive channel at the surface.

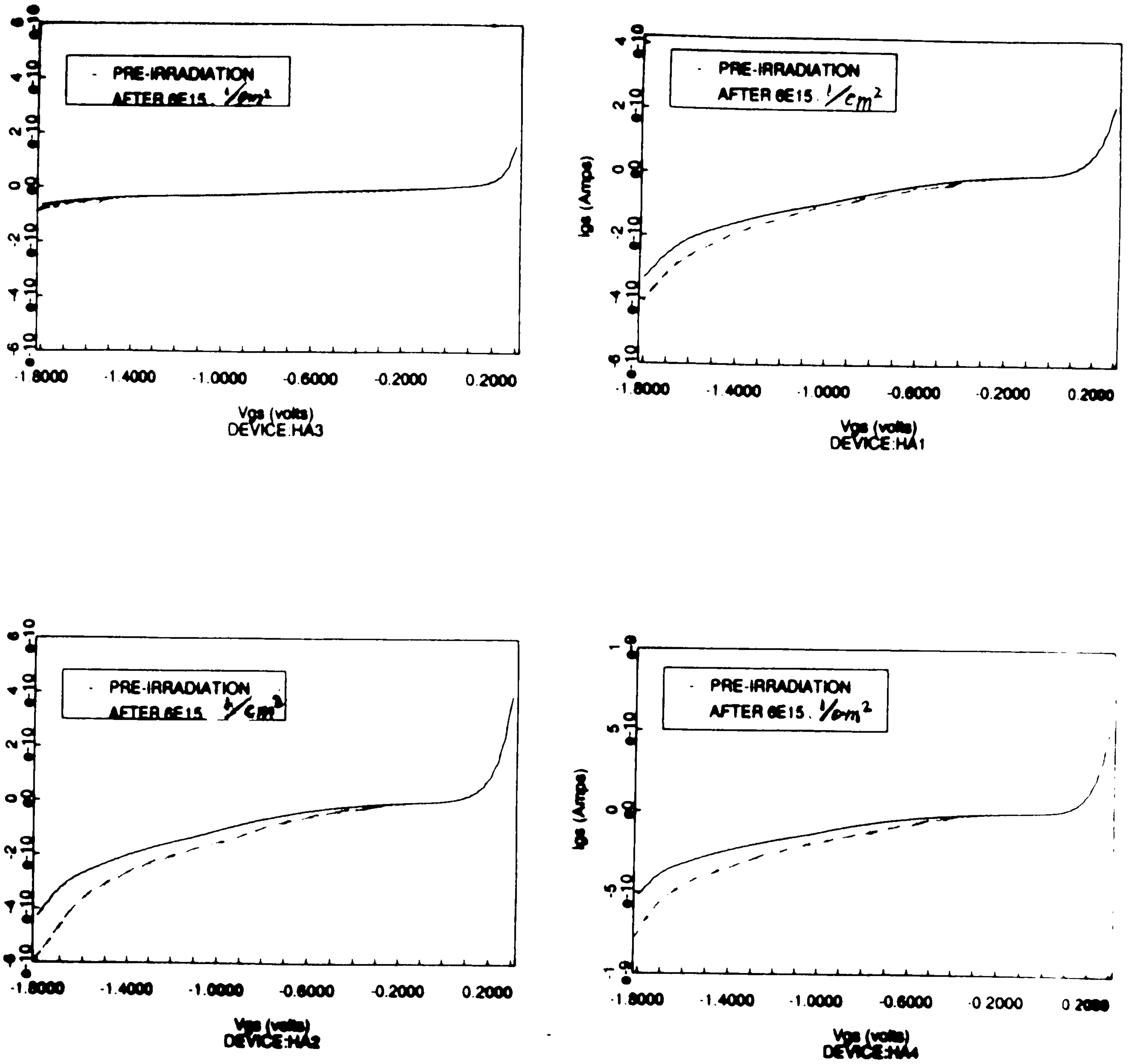

DEVICE:HA3

DEVICE:HA1

DEVICE:HA2

DEVICE:HA4

Figure 22. I_{gs} versus V_{gs} before and after irradiation with 2.5MeV electron (Electron Fluence = $\phi=6X10^{15}$).

6. CONCLUSION

The degradation in the DC characteristics of the AT&T Depletion mode HFET due to electron irradiation has been evaluated.

The threshold voltage becomes more positive after irradiation. The positive threshold voltage shifts have been shown to be dominated by an increase in the net negative charge in the GaAs region due to the filling of radiation induced traps and by an increase in the quantized energy levels and Fermi level at the AlGaAs-GaAs interface at threshold. The traps in the AlGaAs region has been shown not to contribute much to the threshold voltage shifts. The AlGaAs region is depleted and many of the traps in this region are empty therefore not contributing any additional space charge.

The Peak transconductance of the 2DEG have been shown to decrease after irradiation. A decrease in the saturation velocity in the 2DEG and the trapping of electrons otherwise available for conduction are the cause of the decrease in the transconductance. Measurements were not made to quantify the extent of degradation from the two mechanisms.

The drain current in the saturation region is also directly dependent on the saturation velocity and the threshold voltage. It has been shown that at high electron fluence levels ΔV_{th} is the dominant cause in the reduction of the drain saturation current.

The reverse gate leakage current only increased slightly after irradiation. A trend in the reverse gate leakage current has been observed: ΔI_{gs} is directly proportionly to I_{gso} where I_{gso} is the reverse leakage current before irradiation.

This experiment sets the foundation for future experiments aimed at modeling the electron irradiation effects in AT&T HFETs. Although not a comprehensive study of electron irradiation effect in HFETs, it investigates the first order effects using qualitative and quantitative analysis.

BIBLIOGRAPHY

1. D. Pons et al, "Energy Dependence of Deep Level Introduction in Electron Irradiated GaAs, Journal of Applied Physics , 51(4), (1980), 2038.

2. K. Park and K.D. Kwack, " A Model for the Current-Voltage Characteristics of MODFET's", IEEE Trans. Electron Devices , vol. ED-33, no. 5. pp. 673-676, May 1986.

3. M. Yamaguchi and C. Uemura, " Changes in the Electrical Properties of GaAs Due to Electron Irradiation" , Journal of Applied Physics , 57(2), pp. 604-606, Jan. 1985.

4. D. Delagebeaudeuf and N. Linh," Metal-(n) AlGaAs-GaAs two-dimensional electron gas FET", IEEE Trans. Electron Devices , vol. ED-29, no. 6. pp. 955-960,June 1982.

5. K. Lee et al, " Current-Voltage and Capacitance-Voltage Characteristics of Modulation-doped Field-Effect Transistors", IEEE Trans. Electron Devices , vol. ED-30, no. 3. pp. 207-212, March 1983.

6. Lang, D.V. 1976. "Review of Radiation-Induced Defects in III-V Compounds." In Radiation Effects in Semiconductors , edited by N.B. Urli and J.W. Corbett. New York: The Institute of Physics.

7. Krantz, R.J., W.L. Bloss, and M.J. O'Loughlin. 1988. "High Energy Neutron Irradiation Effects in GaAs Modulation-Doped Field Effect Transistors Threshold Voltage." Paper presented at the 1988 annual Nuclear and Space Radiation Effects Conference, Portland Oregon, 11-15 July.

8. McLean, F.B. and T.R. Oldham. 1987. " Basic Machanisms of Radiation Effects in Electronic Materials and Devices." Paper presented at the 1987 annual Nuclear and Space Radiation Effects Conference, Snowmass Co.,July.

9. Anderson,W.T., A. Meulenberg, and S.D. Mittleman. 1987. "Total Dose Ionizing Radiation Measurements of GaAs Devices." Paper presented at the 1987 annual GaAs Reliability Workshop, Portland OR., Oct.

10. Shur, Michael. 1987.
GaAs Devices and Circuits. New York:Plenum Press.

VITA

Steven B. Witmer received a **B.S.E.E.** degree from University of Florida in 1982. After graduation he joined IBM as a staff engineer designing and testing PC peripherals. In 1984 he joined AT&T Microelectronics working on high voltage, optoelectronics and GaAs technologies. His current position is as a Member of Technical Staff with Bell Laboratories in Reading Pa. working in the GaAs Reliability and Radiation Effects Group. His primary responsibility is in testing and modeling radiation effects in GaAs circuits and devices.